Ricci Time in Lemaître-Tolman Model and Block Universe

By:

Yasser Elmahalawy

Supervisor:

Prof. Charles Hellaby

Co-supervisor:

Prof. George Ellis

Minor Dissertation presented in partial fulfilment of the requirements for the degree of Master of Science

in the

Department of Mathematics and Applied Mathematics

University Of Cape Town

November 2014

Declaration of Authorship

I, Yasser Elmahalawy, know the meaning of plagiarism and declare that all of the work in the document, save for that which is properly acknowledged, is my own.

Signed: _____

Date: _____

Abstract

It is common to think of our universe according to the "block universe" idea, which says that spacetime consists of many "stacked" 3-surfaces varied as a function of some kind of proper time τ. Standard ideas do not distinguish past and future, but Ellis' "evolving block universe" tries to make a fundamental distinction. One proposal for this proper time is the proper time measured along the timelike Ricci eigenlines, starting from the big bang. The main idea of this work is to investigate the shape of the $\{\tau = \text{constant}\}$ surfaces relative to the the null surfaces, and determine what makes these surfaces timelike or spacelike. We use the Lemaître-Tolman metric as our inhomogeneous spacetime model, and we find the necessary and sufficient conditions for these $\{\tau = \text{constant}\}$ surfaces to be spacelike or timelike. Furthermore, we indicate whether or not timelike surfaces appear inside black holes and other strong gravity domains, by determining the location of the timelike regions relative to the apparent horizon. Based on this idea, we find that the regions where these surfaces become timelike are often close to the apparent horizons, but always outside them, and in particular timelike regions occur outside black holes. They are always spacelike near the big bang, and at late times (near the crunch or the extreme far future), they are only timelike under special circumstances.

Acknowledgements

All praises to Allah who grant me the strength to complete this thesis in a better way. I would like to express my deep thanks to my supervisor Professor Charles Hellaby for his kind assistant and guidance. I really appreciate his effort to develop my numerical skills as he taught me Maple and Matlab. I would like to thank him for his valuable ideas.

I would like to express my sincere gratitude to my co-supervisor Professor George Ellis for giving me the opportunity to work under his supervision. I also thanks him for his helpful comments and valuable suggestions during my research.

I would like to thank National Astrophysics and Space Science Program and National research Foundation of South Africa for granting me a bursary to complete my Masters degree. Many thanks and appreciation to my family and my wife for supporting to complete my postgraduate studies.

Contents

List of Figures

List of Tables

Abbreviations

BU	**B**lock **U**niverse
EBU	**E**volving **B**lock **U**niverse
CBU	**C**rystallizing **B**lock **U**niverse
LT	**L**emaître **T**olman
FLRW	**F**riedman-**L**emaître-**R**obertson-**W**alker
AH	**A**pparent **H**orizon

Chapter 1

Introduction

There are numerous theories that discuss the nature of time and the way to measure time. Rovelli [1] and Barbour [2] assumed that time does not exist and does not "roll on", according to the idea of standard block universe. Davies [3] proposed that time is real but flow is not. Ellis [4] examined the various views and argued that time exists and its flow is real, calling this the evolving block universe (EBU).

The idea of a block universe [5–7] was proposed by Price [8] and Barbour [2]. This representation denies that time passes and embodies the idea that the flow of time is an illusion [5] and time does not really "roll on". An alternative is the idea of an evolving block universe, enabling one to envisage the flow of time and give a clear picture of a universe where things change [9]. This idea allows us to contemplate the different natures of the past and future, and differentiate between them in our spacetime representation. Moreover, it shows how to indicate the present "now" in the spacetime diagram.

We briefly summarize the evolution of this theory, based on either classical mechanics [10] or quantum mechanics [11], and supported by aspects of General Relativity [12, 13]. The main issue we address is Ellis's concept [4] of how to characterize a preferred time in a curved spacetime.

The standard "classical" block universe assumes that spacetime is fixed, which implies that the past and future are not distinct in this view. This means that space and time are merely coordinates on an unchanging spacetime entity, and the present has no identifying features in this picture. Because of causal determinism, the whole of the past and future can be determined from data given on any arbitrary Cauchy surface. This picture is based on time-reversible local physics and ignores the issue of quantum measurement and related considerations [14].

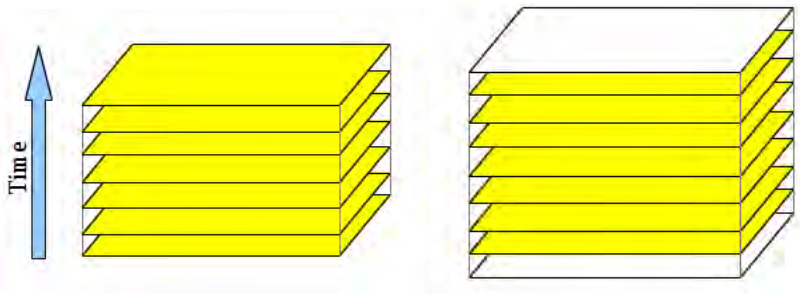

(A) Newtonian spaces (B) Newtonian space-time

FIGURE 1.1: The Newtonian version of the Block Universe.

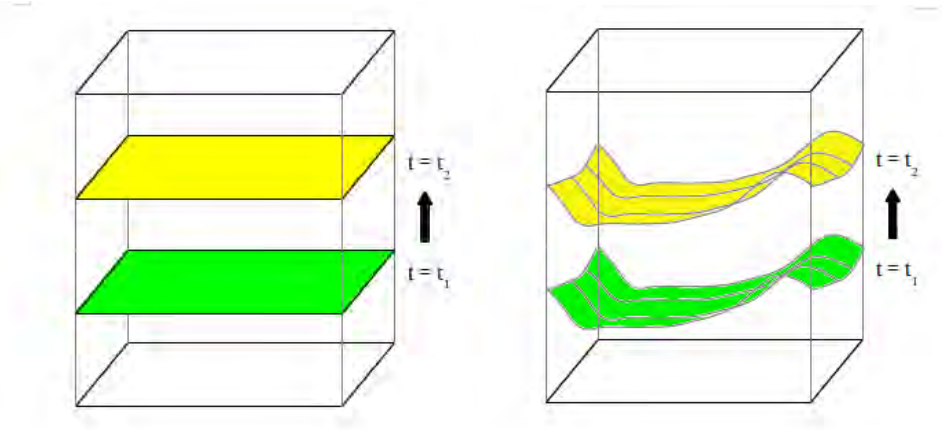

(A) The Special Relativity version of the BU.

(B) The General Relativity version of the BU.

FIGURE 1.2: Block Universe.

There are versions of the block universe picture based in Newtonian mechanics, Special Relativity, and General Relativity. Figure 1.1 represents the Newtonian block universe, where surfaces of constant time are stacked together to form a Newtonian spacetime. We can determine the evolution of physics through the whole spacetime from the initial data at any time surface [14]. Figure 1.2a shows the Special Relativity version of the idea of a block universe, where again surfaces of constant time at different times are represented together to form a single fixed spacetime, with the past and future uniquely determined by the data at any chosen time. "The warrant for this view is the existence and uniqueness theorems for the relevant fields on a fixed Minkowski background spacetime; like, the existence and uniqueness theorems for fluid flows, for Maxwell's equations, or for the Klein Gordon equation" [13–15]. . Figure 1.2b shows the General Relativity versions of the idea of block universe where "the warrant is the existence and uniqueness theorems of general relativity for suitable matter fields" [12, 14].

Ellis emphasised that the idea of a block universe is based on time-reversible microphysical laws, rather than time-irreversible macro-physical laws. He found that time does "roll on" when coarse-graining and emergent effects such as biology are considered. The block universe

idea assumes that we can predict the nature of the future and past using any constant time surface for a simple system, because the equations of state are so easy and ignore friction and dissipative effects, hierarchical structures, feedback effects, or the causal efficacy of information [14].

Ellis [16] suggested that this model does not represent a realistic view of the real universe. He modified the idea of a block universe by considering quantum effects like uncertainty and the effect of wavefunction collapse when measurements take place. This suggests that the idea of a block universe does not work and should be replaced by an Evolving "Emergent" Block Universe ('EBU'). It is based on time-irreversible macroscopic laws and the uncertainty of Quantum mechanics [17].

To visualize the idea of an EBU, consider the following scenario [14]. A massive object has been launched, and is allowed to move either left or right as shown in Figure 1.3. Its motion is controlled by using a computer that fires rocket engines in response to the random decays of a radioactive element [11]. According to the basic nature of quantum uncertainty, the path of the object is then not determined until it happens, which is in total contradiction with the classical view in which we can determine what will happen in the future from the initial data at any previous time.

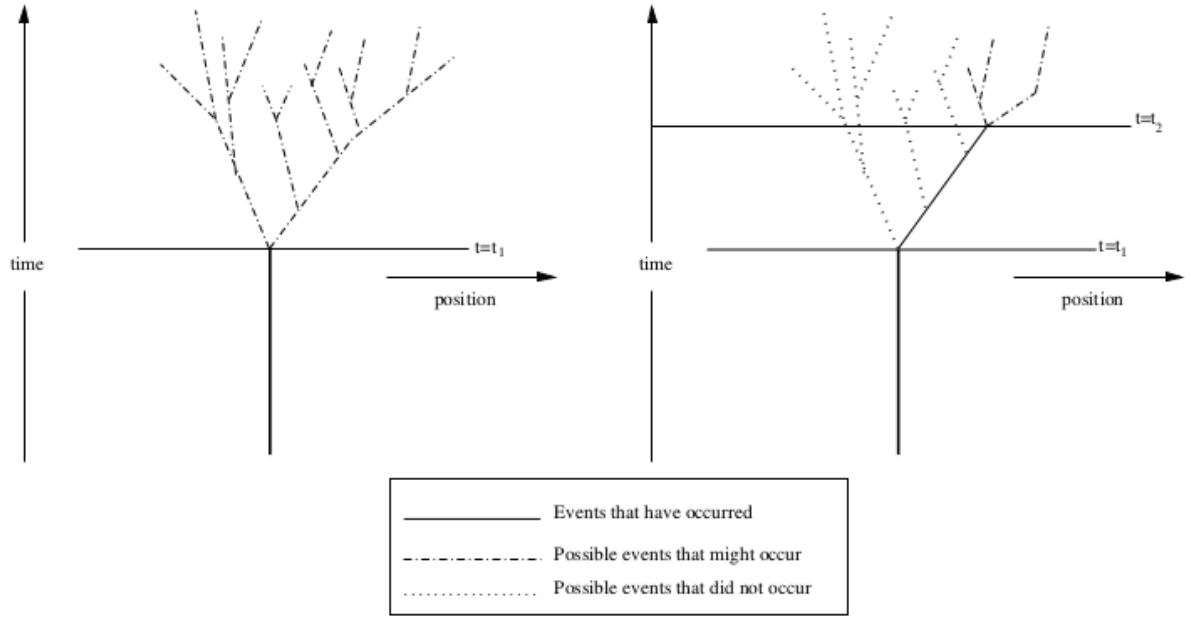

FIGURE 1.3: The world line of a particle whose motion is controlled in a random way, so that what happens is determined only as it happens.

This means that the future, according to the EBU, is uncertain because it is undetermined. The nature of the past is quite different from the future. The past has already happened, but even though our knowledge about it is perhaps lacking, it is fixed and immutable. Furthermore, the spacetime structure changes from indeterminate to definite instant by instant [16].

Let us discuss this proposal in the contexts of Newtonian spacetime and General Relativity. The Newtonian case is usually considered to be an evolving spacetime changed from indefinite to determinate as time passes, as shown in Figure 1.4a. The past is fixed and immutable. The present exists and is unique, but if quantum theory holds the events in it are uncertain. The future is consequently unknown and mutable, and events in it can be influenced by present-day events, even though the spacetime itself is immutable and unchanging.

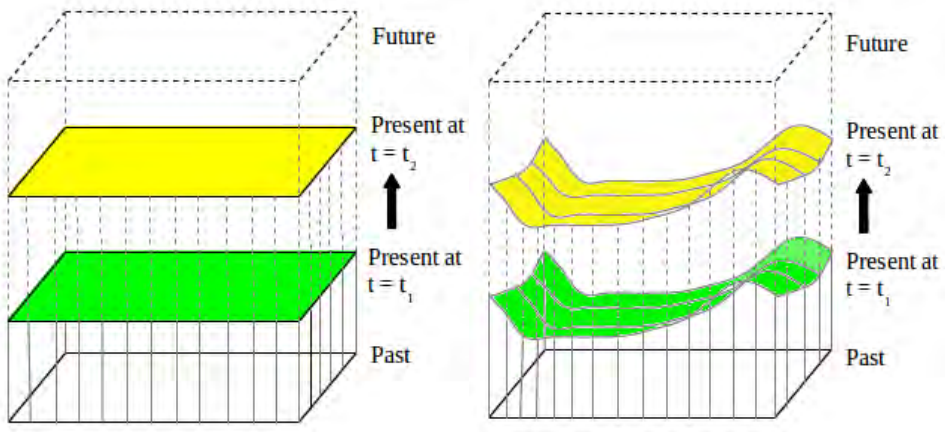

(A) The EBU from the Newtonian and Special Relativity viewpoints

(B) The EBU from the General Relativity viewpoint

FIGURE 1.4: The Evolving Block Universe.

In the General Relativity case by contrast, there is an evolving curved spacetime changed from indefinite to determinate as time passes as shown in Figure 1.4b. It represents the present as the locus where events change from indeterminate to definite, but the future is uncertain until it is determined at successive later times. This case is similar to to the Newtonian case except the spacetime structure itself is curved and undetermined until the present time.

Ellis and Rothman [16] modified the idea of the EBU to give a clear picture of a spacetime where foundational features of quantum mechanics are taken seriously, features that indicate there is sometimes a kind of causation reaching back into the past. A model taking this into account is known as the Crystallizing Block Universe ("CBU"). When quantum effects are significant, the EBU is replaced by the CBU, in which the present time, where the transition take place, can have domains that remain unfixed for some time after events, in general, have moved on.

According to the EBU, the universe consists of a sequence of curved surfaces, labelled as a function of proper time τ, which is measured along chosen timelines $x^i(v)$, determined from the metric tensor $g_{ij}(x^k)$ by [14, 18]

$$\tau = \int \sqrt{-ds^2} = \int \sqrt{-g_{ij}(dx^i/dv)(dx^j/dv)}dv. \tag{1.1}$$

Ellis [4] argued that the present time surface at proper time τ is the surface of $\{\tau = constant\}$ defined in this way, which can be measured by integration along a family of fundamental world lines from the start of the universe to the present day. The fundamental world lines used in this definition are chosen to be the Ricci eigenlines, which represent the average motion of matter, and will be well defined in all realistic spacetimes, because of the existence of an all-pervading cosmic blackbody radiation in the universe.

This prescription defines a family of surfaces that may be locally either spacelike, null, or timelike. The main idea of this thesis is to examine the behavior of the $\{\tau = constant\}$ surfaces $S(\tau_c)$ and find out their nature: are they locally spacelike, timelike, or null? This is an interesting geometric question that can be asked independently of whether one accepts the idea of an evolving block universe or not. One might expect that these surfaces will be spacelike except in the case of very intense gravitational fields. We will show, by investigating these surfaces in a number of Lemaître-Tolman models, that this is not necessarily the case.

The Lemaître-Tolman metric is a model for studying the possibility of an inhomgeneous universe [19–21], or of structures within it. It is very similar to dust Robertson-Walker model, in that it is spherically symmetric and comoving, but Lemaître-Tolman models are generally inhomogeneous in the radial direction. It was first proposed by Lemaître [22] in 1933 and then Tolman [23] in 1934. A few years later, Bondi [24] investigate this model again in 1947. (It is sometimes called the "Tolman model", and sometimes the "Lemaître-Tolman-Bondi model".)

The Lemaître-Tolman model is a spherically symmetric dust model, which is widely used for both large and small scales. Because it is an exact solution, it is good for studying the non-linearity of Einstein field equations [25]. It has a lot of success in describing the expansion or collapse of structures of the whole universe under gravity. It gives a proper physical interpretation for many observations [26–29]. Interestingly, it can be used to describe a homogeneous cosmology in one limit, and non-vacuum black holes in another limit [30, 31].

Chapter 2

The Lemaître Tolman Model and its Evolution

On a large scale, the Robertson-Walker metric [1] has had much success in giving a physical interpretation of many phenomena that occurred in our universe, such as the existence of the cosmic background radiation, but of course it fails on a small scale [12]. An alternative approach using the Lemaître-Tolman model, first proposed by Lemaître in 1933, assists in studying the inhomogeneity and non-linearity of the Einstein field equations. The Lemaître-Tolman metric is a dust model which is spherically-symmetric, but inhomogeneous in the radial direction [19]. There are several different inhomogeneous metrics such as the Lemaître-Tolman and Szekeres metrics [20]. In this chapter, we are concerned only with the first metric.

2.1 Lemaître-Tolman Model

The Lemaître-Tolman metric is written in synchronous, comoving coordinates,

$$ds^2 = -dt^2 + \frac{(R')^2}{1+f}dr^2 + R^2(d\theta^2 + \sin^2\theta d\phi), \tag{2.1}$$

where R is the areal radius, $f(r)$ is a free function determining the local geometry and $R^{'} = \partial R/\partial r$. The matter is a pressure-free perfect fluid [32], and the energy momentum tensor is defined by

$$T^{ab} = \rho u^a u^b, \tag{2.2}$$

[1] Based on the homogeneity and isotropy of the universe

where ρ is the mass-energy density, and u^a is the fluid's four velocity, which is defined as

$$u^a = \delta^a_t, \tag{2.3}$$

since the spatial coordinates are comoving with the matter [29]. The solution of the Einstein field equations (see appendix A) gives the evolution equation

$$\dot{R}^2 = \frac{2M(r)}{R} + f(r), \tag{2.4}$$

where $M(r)$ is the gravitational mass within the comoving shell of radius r, and $f(r)$ has a second interpretation as $2E(r)$ which is twice the local energy per unit mass of the dust particles. Also, from solving the Einstein field equations, the density is given by

$$\kappa\rho = \frac{2M'}{R^2R'}. \tag{2.5}$$

The Kretschmann scalar [19] is an invariant measure of spacetime curvature which is given by

$$\mathcal{K} = R_{abcd}R^{abcd} = \frac{48M^2}{R^6} + \frac{32MM'}{R^5R'} + \frac{12(M')^2}{R^4(R')^2}. \tag{2.6}$$

Note that $\mathcal{K}$ only diverges where R or R' are zero, while M and M' are not. Similarly, ρ only diverges where M'/R' is zero. The solutions of equation (2.4), when the cosmological constant Λ is zero, are of 3 types, depending on the value of f (or more correctly, the value of $f/M^{3/2}$),

- Hyperbolic, $f > 0$

$$R = \frac{M}{f}(\cosh\eta - 1), \qquad (\sinh\eta - \eta) = \frac{f^{3/2}(t-a)}{M}; \tag{2.7}$$

- Parabolic, $f = 0$:

$$R = M\left(\frac{\eta^2}{2}\right), \qquad \left(\frac{\eta^3}{6}\right) = \frac{(t-a)}{M}; \tag{2.8}$$

- Elliptic, $f < 0$:

$$R = \frac{M}{(-f)}(1 - \cos\eta), \qquad (\eta - \sin\eta) = \frac{(-f)^{3/2}(t-a)}{M}; \tag{2.9}$$

where $a(r)$ is the local time of the big bang, i.e. the time on each worldline at which $R = 0$. These are very like the 3 Robertson-Walker cases; the hyperbolic evolution is like the open, ever-expanding, $k = -1$ model, the elliptic case is like the closed, expanding and re-collapsing,

$k = +1$ model, and the parabolic solution is like the borderline $k = 0$ model.[2] Consequently the parabolic case will not be investigated explicitly in this thesis. The 3 arbitrary functions of this model each contribute to its inhomogeneity. The contained mass $M(r)$ can increase with r rapidly, slowly, or even stay constant over some range of r. The local geometry/energy function $f(r)$ typically increases with radius, but can increase slowly or rapidly. Lastly the bang time does not have to be the same for each worldline. Usually outer shells of matter "explode" off the initial singularity at earlier times. The parameter η can be thought of as giving the stage of evolution, such as "early", "intermediate", and "late". The 3 types of solution are not mutually exclusive, and it is possible to have a hyperbolic region outside and elliptic region, with a parabolic locus at the boundary between them. This models gravitational collapse in an expanding universe [33, 34].

Parametric expressions for the evolution of R' (see appendix B) will be very useful for deriving the conditions for no shell crossings [35] and moreover, we will use these expressions to calculate the radial null slopes for both elliptic and hyperbolic cases in chapter 3. These expressions can be derived from equations (2.7) and (2.9) which are

- Elliptic, $f < 0$:

$$R' = \frac{M'}{(-f)}\psi_1 + \frac{Mf'}{f^2}\psi_2 + (-a')\sqrt{(-f)}\psi_3, \tag{2.10}$$

where

$$\psi_1 = \frac{2 - 2\cos\eta - \eta\sin\eta}{1 - \cos\eta}, \tag{2.11}$$

$$\psi_2 = \frac{1}{2}\frac{4 - 4\cos\eta - 3\eta\sin\eta + \sin^2\eta}{1 - \cos\eta}, \tag{2.12}$$

and

$$\psi_3 = \frac{\sin\eta}{1 - \cos\eta}. \tag{2.13}$$

- Hyperbolic, $f > 0$:

$$R' = \frac{M'}{f}\psi_4 + \frac{Mf'}{f^2}\psi_5 + (-a')\sqrt{f}\psi_6, \tag{2.14}$$

[2] However, with the LT model, the geometry is not so strongly tied to the evolution type, as it is in the FLRW model.

where

$$\psi_4 = \frac{2 - 2\cosh\eta + \eta\sinh\eta}{\cosh\eta - 1}, \tag{2.15}$$

$$\psi_5 = -\frac{1}{2}\frac{4 - 4\cosh\eta + 3\eta\sinh\eta - \sinh^2\eta}{\cosh\eta - 1}, \tag{2.16}$$

and

$$\psi_6 = \frac{\sinh\eta}{\cosh\eta - 1}. \tag{2.17}$$

A scale length and time, characteristic for each worldline, are defined as

$$\tilde{R}(r) = \frac{M}{|f|}, \tag{2.18}$$

and

$$\tilde{T}(r) = \frac{M}{|f|^{3/2}}, \tag{2.19}$$

respectively. Note that the life time from the bang to crunch in elliptic models is $2\pi\tilde{T}$.

2.2 Special Cases

The Lemaître-Tolman model has several interesting special cases; the first two below are of particular interest for the thesis.

- **Dust Robertson-Walker**: This occurs when

$$M = M_0 r^3, \qquad f = -kr^2, \qquad a^{'} = 0. \tag{2.20}$$

- **Schwarzschild**: If $M' = 0$, then we have at least part of the vacuum spherical spacetime. To get the full Schwarzschild-Kruskal-Szekeres (SKS) spacetime, requires an elliptic region, and a worldline where $f = -1$ and $a' = f' = 0$ at which $R' = 0$, a' is maximum, and f' and R' are minimum. One may easily construct a non-vacuum black hole with the same geomtry and topology, if M' is made non-zero and minimum at $f = -1$ [30, 36].

- **Datt-Kantowski-Sachs**: There is a well-behaved limit of the Lemaître-Tolman model, occuring if $R^{'} = 0$ and $f = -1$ globally [36].

- **Vaidya**: With appropriate transformations, the limit of infinite local energy $f \to \infty$ gives a model in which the "matter" worldlines are null. For this to work, the initial Lemaître-Tolman model needs to be hollow with vacuum at the centre [37, 38].

2.3 Origins

An origin occurs where $R(r_0, t) = 0$ for all t on a particular worldline, r_0 [39]. This implies that all time derivatives of R along r_0 are also zero. Normally $r_0 = 0$. Obviously, even at the origin, t must vary over a finite or infinite range, and so must the parameter η. So it is clear from equations (2.7) and (2.9) that, $M/|f|^{3/2}$ must remain finite and non-zero in the limit as $r \to r_0$, and $M/|f|$ must go to zero to make R zero. Therefore, $M \sim |f|^{3/2}$ in the neighbourhood of the origin, and both M and f go to zero there. But this does not mean that the time evolution is parabolic [21]. When doing numerical calculations, we need to avoid calculating zero over zero, so for each choice of arbitrary functions, we need to separately calculate the origin limits of several different expressions. As an example, consider the following arbitrary functions

$$M = M_0(r^3 + M_1 r^4 + M_2 r^5), \tag{2.21}$$

$$f = -k(r^2 + f_1 r^3 + f_2 r^4), \tag{2.22}$$

where M_0, M_1, M_2, k, f_1, and f_2 are constants. Note that these functions represent the elliptic or hyperbolic case, depending on the sign of the arbitrary function f, where $f \neq 0$, according to equation (2.22). At the origin where $r = 0$, M and f are equal to zero, we need to be able to calculate R and t, for each given η in both elliptic and hyperbolic cases. To avoid the zero-over-zero problem, we re-express equations (2.21) and (2.22) as

$$M = M_0 r^3(1 + M_1 r + M_2 r^2), \tag{2.23}$$

$$f = -k r^2(1 + f_1 r + f_2 r^2). \tag{2.24}$$

so that

$$\left.\frac{M}{f}\right|_{r\to 0} = -\left.\frac{M_0 r(1 + M_1 r + M_2 r^2)}{k(1 + f_1 r + f_2 r^2)}\right|_{r\to 0} = 0, \tag{2.25}$$

and

$$\left.\frac{M}{f^{3/2}}\right|_{r\to 0} = \left.\frac{M_0(1 + M_1 r + M_2 r^2)}{\Big(-k(1 + f_1 r + f_2 r^2)\Big)^{3/2}}\right|_{r\to 0} = \frac{M_0}{(-k)^{3/2}}, \tag{2.26}$$

which means that R and t have a specific value at the origin rather than being undefined or going to infinity. The combinations of arbitrary functions and derivatives in equations (2.10)-(2.19) all require this treatment.

2.4 Regular Extrema

In a spatially closed spherical model, such as the $k = +1$ FLRW model, there must be place where the areal radius is maximum, decreasing on either side towards an origin. This is like the equator and the two poles on the surface of the earth. Similarly, in Lemaître-Tolman models of vacuum and dense black holes, there is a minimum of the areal radius at the "throat" or "neck". Regular extrema in LT models occur if $R' = 0$ at one or more particular r_m values without the density or curvature diverging and without a shell crossing forming [35]. This means that

$$R'(t, r_m) = 0 \qquad \forall\ t \tag{2.27}$$

The conditions for a regular maximum or minimum [31] without shell crossings or surface layers are

$$M'(r_m) = f'(r_m) = a'(r_m) = 0, \qquad f(r_m) = -1 \tag{2.28}$$

2.5 Singularities

A singularity is a location where the Einstein equations break down [12]. This occurs due to the divergence of density equation (2.5) or the Kretschmann scalar equation (2.6) in the Lemaître-Tolman model. This model has several different singularities.

1. **Big Bang** : This is considered to be one of the main singularities of the Lemaître-Tolman model. This occurs on each worldline, in both elliptic and hyperbolic cases, where $t = a$, causing $R(a, r) = 0$ for all r. The big bang 3-surfaces are space-like [21] as will be seen in chapter 3. In contrast an origin is timelike. This Lemaître-Tolman big bang is similar to the FLRW big bang, except it does not need to be simultaneous.

2. **Big Crunch** : This occurs in elliptic models only, where $t = a + 2\pi\tilde{T}$, also causing $R = 0$ on each worldline, and these surfaces are also space-like [19]. Note that both big bang and crunch are singular due to the divergence of the density equation (2.5) and curvature equation (2.6).

3. **Shell Crossings** : These singularities occur due to the collision between an inner and an adjacent outer shell of constant r [35] where $R^{'} = 0$. They represent a break down in the Lemaître-Tolman assumptions. These surfaces have an infinite density, with a positive density on the 'near' side, while the region 'behind' them has a negative density, which is physically unacceptable. The shell-crossing surfaces are time-like, which makes them totally different from the big bang and crunch surfaces. Moreover, they have a different redshift structure and surface density from the big bang. Shell crossings can be avoided by applying certain conditions on the arbitrary functions which will be discussed in §2.6. They do not remain at constant r, and are distinct from the regular extrema mentioned above, which are not singular, i.e. the density ρ does not diverge.

4. **Shell Focusing** : This can occur on the central worldline (origin), at the moment of the big crunch. Under certain conditions, many light rays can be emitted from this one point on the crunch can even travel to infinity, rather than being captured by the crunch [40–44]. The nature of this singularity and its physical origin are very difficult to understand.

2.6 Avoiding Shell Crossings

Shell crossing singularities would be extremely common if the 3 arbitrary functions in the Lemaître-Tolman model were chosen at random. They happen at loci where $R' = 0$ that aren't regular extrema as explained in §2.5 and §2.4. The main idea of this section is to show how to avoid shell crossings from occurring in our Lemaître-Tolman models, by applying certain conditions, since we want our models to be free of serious irregularities. Now, let us derive the necessary and sufficient conditions for no shell crossings to occur at any time in an Lemaître-Tolman model, for elliptic and hyperbolic evolution, separately.

2.6.1 Elliptic Regions:

Equation (2.10) can be written as

$$R' = p_1\psi_1 + q\psi_2 + (-a')\sqrt{(-f)}\psi_3, \tag{2.29}$$

where p_1, q are given by

$$p_1 = \frac{M'}{(-f)}, \qquad q = \frac{Mf'}{f^2}. \tag{2.30}$$

We will consider regions where $R' \geq 0$, and the $R' \leq 0$ case then follows in the obvious way. It is obvious from equation (2.5) that positive density needs $M' \geq 0$ where $R^{'} \geq 0$. Figure 2.1 indicates the behavior of ψ_1, ψ_2 and ψ_3 as functions of η.

At early times ($\eta \to 0$), we find that

$$\psi_1 = \frac{\eta^2}{6} + \frac{\eta^4}{360} + \frac{\eta^6}{15120} + \cdots \approx \frac{\eta^2}{6}, \tag{2.31}$$

$$\psi_2 = \frac{\eta^4}{40} - \frac{\eta^6}{1680} + \frac{\eta^8}{67200} + \cdots \approx \frac{\eta^4}{40}, \tag{2.32}$$

$$\psi_3 = \frac{2}{\eta} - \frac{\eta}{6} - \frac{\eta^3}{360} + \cdots \approx \frac{2}{\eta}, \tag{2.33}$$

and thus equation (2.29) reduces to

$$R' = p_1 \frac{\eta^2}{6} + q\frac{\eta^4}{40} + (-a')\sqrt{(-f)}\frac{2}{\eta} \approx (-a')\sqrt{(-f)}\frac{2}{\eta}. \tag{2.34}$$

Note that the third term in equation (2.34) is dominant compared to the first and second terms, provided $a' \neq 0$. This means that $a' \leq 0$ for $R^{'} \geq 0$.

At late times ($\eta = 2\pi - \delta$ and $\delta \to 0$), we find that

$$\psi_1 = \frac{4\pi}{\delta} - \frac{\pi\delta}{3} + \frac{\delta^2}{6} + \cdots \approx \frac{4\pi}{\delta}, \tag{2.35}$$

$$\psi_2 = \frac{6\pi}{\delta} - \frac{\pi\delta}{2} - \frac{\pi\delta^3}{120} + \cdots \approx \frac{6\pi}{\delta}, \tag{2.36}$$

$$\psi_3 = -\frac{2}{\delta} + \frac{\delta}{6} + \frac{\delta^3}{360} + \cdots \approx -\frac{2}{\delta}, \tag{2.37}$$

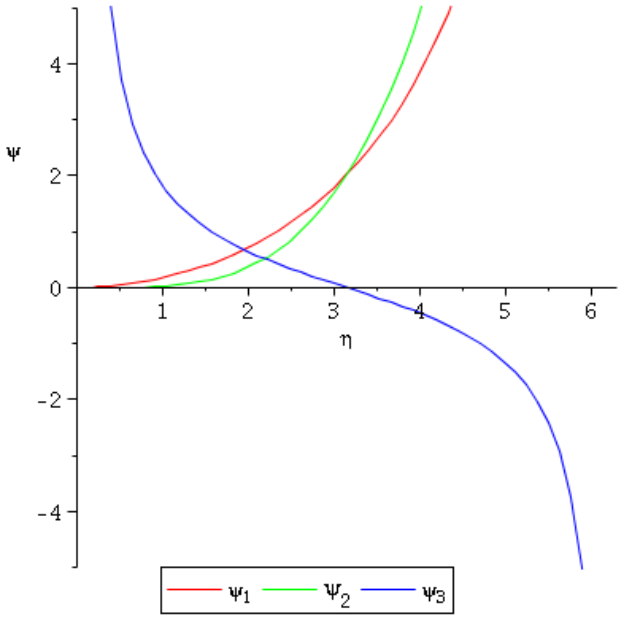

FIGURE 2.1: The shape of the functions ψ_1, ψ_2 and ψ_3 for the elliptic case, $0 \leq \eta \leq 2\pi$, showing early and late time behaviour.

so that equation (2.29) reduces to

$$R' = \frac{4\pi}{\delta}\frac{M'}{(-f)} + \frac{6\pi}{\delta}\frac{Mf'}{f^2} + \frac{2a'}{\delta}\sqrt{(-f)}. \tag{2.38}$$

Since $R' > 0$, we find that

$$a' \geq \frac{2\pi M}{(-f)^{3/2}}\left(\frac{M'}{M} - \frac{3f'}{2f}\right) = 2\pi\tilde{T}', \tag{2.39}$$

which implies that

$$\frac{M'}{M} \geq \frac{3f'}{2f}. \tag{2.40}$$

2.6.2 Hyperbolic Regions:

Equation (2.14) can be written as

$$R' = p_2\psi_4 + q\psi_5 + (-a')\sqrt{f}\psi_6, \tag{2.41}$$

where p_2 is given by

$$p_2 = \frac{M'}{f}. \tag{2.42}$$

As above, we assume $R' \geq 0$, and it is clear from equation (2.5) that $M' \geq 0$ must hold for positive density. Figure 2.2 indicates the behavior of ψ_4, ψ_5 and ψ_6 as functions of η.

At early times ($\eta \to 0$), we find that

$$\psi_4 = \frac{\eta^2}{6} - \frac{\eta^4}{360} + \frac{\eta^6}{15120} + \cdots \approx \frac{\eta^2}{6}, \tag{2.43}$$

$$\psi_5 = \frac{\eta^4}{40} + \frac{\eta^6}{1680} + \frac{\eta^8}{67200} + \cdots \approx \frac{\eta^4}{40}, \tag{2.44}$$

$$\psi_6 = \frac{2}{\eta} + \frac{\eta}{6} - \frac{\eta^3}{360} + \cdots \approx \frac{2}{\eta}. \tag{2.45}$$

Thus, equation (2.41) reduces to

$$R' = p_2\frac{\eta^2}{6} + q\frac{\eta^4}{40} + (-a')\sqrt{f}\frac{2}{\eta} \approx (-a')\sqrt{f}\frac{2}{\eta}, \tag{2.46}$$

showing the third term in equation (2.46) is dominant compared to the first and second terms, if $a' \neq 0$, and this means that $a' \leq 0$ is required to ensure $R^{'} \geq 0$.

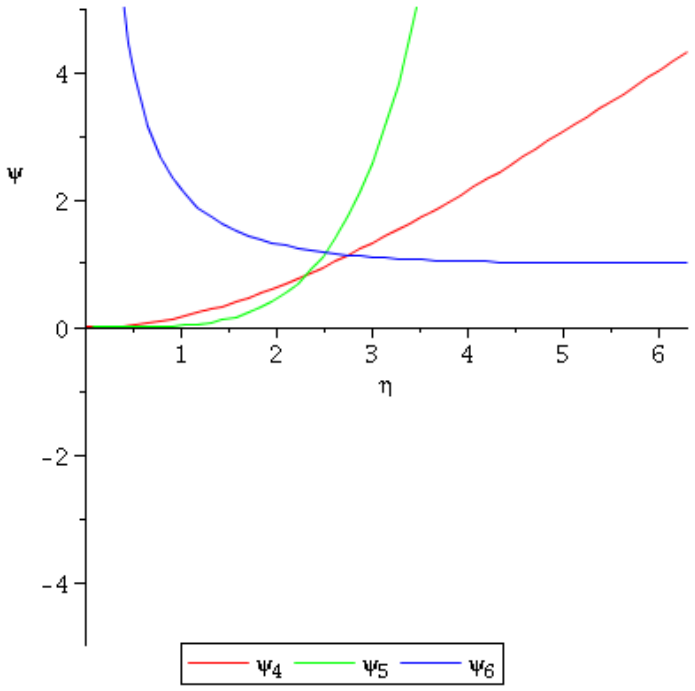

FIGURE 2.2: The shape of the functions ψ_4, ψ_5 and ψ_6 for the hyperbolic case, $0 \leq \eta < \infty$, showing early and late time behaviour.

At late times ($\eta \to \infty$), we find that

$$\psi_4 \approx \eta, \qquad \psi_5 \approx \frac{e^\eta}{4}, \qquad \psi_6 \approx 1 + 2e^{-\eta}. \tag{2.47}$$

This means that the second term in equation (2.41) is dominant compared to the first and third term and equation (2.41) reduces to

$$R' \approx \frac{M'}{f}\eta + \frac{Mf'}{4f^2}e^\eta \approx \frac{Mf'}{4f^2}e^\eta, \tag{2.48}$$

meaning that $f' \geq 0$ is required. Note that the conditions for no shell crossings for the parabolic case are similar to those for the hyperbolic case. Finally, we can summarize the no-shell-crossing conditions in table 2.1.

2.7 Scaled Conformal Time

Below we will numerically calculate and plot results for a number of explicit models, and they will display a specific range of t and r values. The evolution calculations will be based on the conformal time η, so it will be necessary to set a suitable range of η and to have sufficient data points in that range to make a good plot. The relation between t and η depends on the scale time $\tilde{T}$, as shown by equations (2.7), (2.9) and (2.19). In addition, near parabolic regions, where f passes through zero, it can be seen that $f \to 0$ in equations (2.7) and (2.9) implies

Conditions for No Shell Crossings		
$R^{'}$	f	$M^{'}$, $f^{'}$, $a^{'}$
> 0	≥ 0	$M^{'} \geq 0$ $f^{'} \geq 0$ $a^{'} \leq 0$ but not all 3 equalities at once
	< 0	$M^{'} \geq 0$ $2\pi\tilde{T}^{'} + a^{'} \geq 0$ $a^{'} \leq 0$ but not all 3 equalities at once
$= 0$	$= 0$	$M^{'} = 0$ $f^{'} = 0$ $a^{'} = 0$
< 0	≥ 0	$M^{'} \leq 0$ $f^{'} \leq 0$ $a^{'} \geq 0$ but not all 3 equalities at once
	< 0	$M^{'} \leq 0$ $2\pi\tilde{T}^{'} + a^{'} \leq 0$ $a^{'} \geq 0$ but not all 3 equalities at once

TABLE 2.1: Conditions for no shell crossings.

$\eta \to 0$. To get a useful parameter in the parabolic case the defintion $\overline{\eta} = \eta/\sqrt{|f|}$ is used before taking the limit $f \to 0$. These two problems are handled numerically by defining the rescaled conformal time as

$$\tilde{\eta} = \frac{f^{1/2}}{M^{1/3}}\eta. \tag{2.49}$$

Chapter 3

Ricci Time Surfaces in LT Model

In the context of the Lemaître-Tolman model, we are next going to calculate the slopes of the surfaces $S(\tau_c)$[1] and the slopes of the radial null rays, and find the ratio between them. This ratio allows us to determine whether each $S(\tau_c)$ is spacelike, null or timelike, for both hyperbolic and elliptic cases. Furthermore, we derive the necessary and sufficient conditions for $S(\tau_c)$ being locally spacelike, null or timelike in different time regions.

3.1 Ricci Time

Ellis [4] argued that the "present" is a surface of constant time, and that the time τ for any $S(\tau_c)$ can be evaluated by integrating proper time along suitable worldlines, starting at the beginning of the universe up to $S(\tau_c)$. Ellis proposed that the paths to use are the Ricci eigenlines, that is the integral paths of the timelike eigenvectors of the Ricci tensor. The resulting time τ will be called the Ricci time. In the Lemaître-Tolman model, the Ricci eigenlines turn out to be the matter worldlines, as shown in appendix A, $u^a = \delta^a_t$, and the proper time is just the local cosmic time since the bang,

$$\tau = t - a. \tag{3.1}$$

Consequently, the slope of $S(\tau_c)$ is simply the derivative of equation (3.1), holding τ constant, i.e.

$$\left.\frac{dt}{dr}\right|_\tau = a'. \tag{3.2}$$

[1] $S(\tau_c)$ is the family of 3-surfaces on which τ is constant, τ being defined in equation (3.1).

This already shows that the slope of the big bang surface is likely to be very significant in these calculations.

3.2 Radial Light Rays & the Spacelike/Timelike Conditions

In this section, we are going to calculate the radial null slope, which we will compare with the slope of $S(\tau_c)$, to obtain the conditions for $S(\tau_c)$ being locally timelike, null or spacelike.

For radial null paths we have, $ds^2 = d\theta^2 = d\phi^2 = 0$, and thus, equation (2.1) leads to

$$\left.\frac{dt}{dr}\right|_n = \pm\frac{R'}{\sqrt{1+f}}, \tag{3.3}$$

where the $+$ sign is used for a radially outgoing null path while the $-$ sign is used for a radially incoming null path. It is clear from the previous chapter that the appropriate exprtession for R' depends on the value of f, so we must consider elliptic and hyperbolic cases seperately. The ratio of the null slope equation (3.3) to the slope of $S(\tau_c)$ equation (3.2) is[2]

$$\mathcal{R} = \frac{|R'|}{|a'\sqrt{1+f}|}. \tag{3.4}$$

Since the slopes of the incoming and outgoing light rays in equation (3.3) have the same magnitude, we only need to compare the magnitudes of equations (3.2) and (3.3). Locally, the surface $S(\tau_c)$ is timelike if it is steeper than the (radial) null path, i.e. $0 < \mathcal{R} < 1$, and conversely it is spacelike if $\infty > \mathcal{R} > 1$. $S(\tau_c)$ is a null surface only if $\mathcal{R} = 1$.

Next let us discuss equations (3.3) and (3.4) in the contexts of hyperbolic and elliptic cases.

1. **Hyperbolic,** $f > 0$: Substituting equation (2.14) into equation (3.3), we get

$$\left.\frac{dt}{dr}\right|_n = \pm\frac{1}{\sqrt{1+f}}\left(\frac{M'}{f}\psi_4 + \frac{Mf'}{f^2}\psi_5 + (-a')\sqrt{f}\psi_6\right), \tag{3.5}$$

   so that the ratio between the null surface slope equation (3.5) and the $S(\tau_c)$ surface slope equation (3.2) is

$$\mathcal{R} = \frac{1}{|a'|\sqrt{1+f}}\left|\frac{M'}{f}\psi_4 + \frac{Mf'}{f^2}\psi_5 + (-a')\sqrt{f}\psi_6\right|. \tag{3.6}$$

   It is clear from equation (3.6) that both the arbitrary functions, and the evolution functions will affect $\mathcal{R}$, and the timelike or spacelike nature of $S(\tau_c)$ is likely to vary with position and time.

[2] It is convenient to put the simpler expression in the denominator.

2. **Elliptic,** $f < 0$: Using equation (2.10), equations (3.3) and (3.4) evaluate to

$$\left.\frac{dt}{dr}\right|_n = \pm\frac{1}{\sqrt{1+f}}\left(\frac{M'}{(-f)}\psi_1 + \frac{Mf'}{f^2}\psi_2 + (-a')\sqrt{(-f)}\psi_3\right) \tag{3.7}$$

and

$$\mathcal{R} = \frac{1}{|a'|\sqrt{1+f}}\left|\frac{M'}{(-f)}\psi_1 + \frac{Mf'}{f^2}\psi_2 + (-a')\sqrt{(-f)}\psi_3\right| \tag{3.8}$$

respectively.

In the successive two sections, we will discuss the conditions, in certain limits, for $S(\tau_c)$ being spacelike, null or timelike, for both hyperbolic and elliptic regions.

3.2.1 Hyperbolic Regions

We found in §2.6 that, at early times ($\eta \to 0$), $\psi_4 \approx (\eta^2/6)$, $\psi_5 \approx (\eta^4/40)$ and $\psi_6 \approx (2/\eta)$. At late times ($\eta \to \infty$), $\psi_4 \approx \eta$, $\psi_5 \to (e^\eta/4)$ and $\psi_6 \approx (1 + 2e^{-\eta})$. The nature of the ψ functions is totally different from one interval time to the other one. Therefore, we separate the entire range of time to three different regions, and we investigate the ratio equation (3.6) for each of these regions :

- At early times ($\eta \to 0$), equations (3.5) and (3.6) reduce to

$$\left.\frac{dt}{dr}\right|_n = \pm\frac{1}{\sqrt{1+f}}\left(\frac{M'}{f}\frac{\eta^2}{6} + \frac{Mf'}{f^2}\frac{\eta^4}{40} + (-a')\sqrt{f}\frac{2}{\eta}\right) \approx \pm\frac{2(-a')}{\eta}\sqrt{\frac{f}{1+f}}, \tag{3.9}$$

  and

$$\mathcal{R} = \frac{1}{|a'|\sqrt{1+f}}\left|\frac{M'}{f}\frac{\eta^2}{6} + \frac{Mf'}{f^5}\frac{\eta^4}{40} + (-a')\sqrt{f}\frac{2}{\eta}\right| \approx \frac{2}{\eta}\sqrt{\frac{f}{1+f}}, \tag{3.10}$$

  respectively, assuming $a' \neq 0$. It is clear that in the limit, equation (3.10) goes to infinity provided $a' \neq 0$, because ψ_6 diverges. This means that $S(\tau_c)$ becomes spacelike because $\mathcal{R}$ is greater than one. If $a' = 0$, then equation (3.10) again goes to infinity because the denominator is equal to zero and $\mathcal{R}$ is divergent. Generally, $S(\tau_c)$ is spacelike everywhere at early enough times.

- At intermediate times we have to deal with the full expression equation (3.6), so it will not be easy to obtain definite analytical results. Since the initial $\mathcal{R}$ is infinite, and timelike $S(\tau_c)$ requires $\mathcal{R} < 1$, it makes sense to look for the minimum of $\mathcal{R}$ as η changes.

Differentiating equation (3.6), we will need the derivatives of ψ_4, ψ_5 and ψ_6. To find an estimate for η_{min}, we differentiate equations (2.15), (2.16) and (2.17) with respect to η, obtaining

$$\frac{d\psi_4}{d\eta} = \frac{-\sinh\eta + \eta\cosh\eta}{\cosh\eta - 1} - \frac{(2 - 2\cosh\eta + \eta\sinh\eta)\sinh\eta}{(\cosh\eta - 1)^2} = \frac{\sinh\eta - \eta}{\cosh\eta - 1}, \tag{3.11}$$

$$\begin{aligned}\frac{d\psi_5}{d\eta} &= -\frac{1}{2}\frac{-2\cosh\eta\sinh\eta - \sinh\eta + 3\eta\cosh\eta}{\cosh\eta - 1} \\ &+ \frac{1}{2}\frac{(4 - 4\cosh\eta + 3\eta\sinh\eta - \sinh^2\eta)\sinh\eta}{(\cosh\eta - 1)^2} = \frac{\sinh\eta}{2} - \frac{3(\sinh\eta - \eta)}{2(\cosh\eta - 1)},\end{aligned} \tag{3.12}$$

and

$$\frac{d\psi_6}{d\eta} = \frac{\cosh\eta}{\cosh\eta - 1} - \frac{\sinh^2\eta}{(\cosh\eta - 1)^2} = \frac{-1}{\cosh\eta - 1}. \tag{3.13}$$

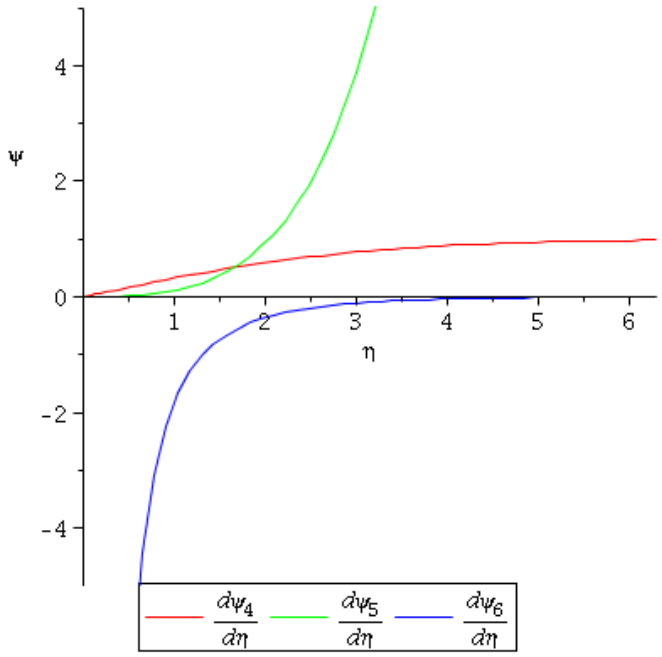

FIGURE 3.1: The shape of $\frac{d\psi_4}{d\eta}$, $\frac{d\psi_5}{d\eta}$ and $\frac{d\psi_6}{d\eta}$ for the hyperbolic case.

Figure 3.1 illustrates the behavior of $\frac{d\psi_4}{d\eta}$, $\frac{d\psi_5}{d\eta}$ and $\frac{d\psi_6}{d\eta}$ for a significant time range. We find that $\frac{d\psi_4}{d\eta}$ is monotonically increasing from 0 to 1, while $\frac{d\psi_5}{d\eta}$ is monotonically increasing from 0 to ∞ and $\frac{d\psi_6}{d\eta}$ is monotonically increasing from $-\infty$ to 0. These η functions are multiplied by functions of r, the same ones as in equation (3.6), so the exact minimum η will be different for each worldline, but if we assume the r functions are of similar magnitudes, then from figure 3.1 we estimate that η_{min} is approximately

1.7. Now, equation (3.6) reduces to

$$\mathcal{R} = \frac{\left|AfM' + BMf' + C(-a')f^{5/2}\right|}{|a'|f^2\sqrt{1+f}}, \tag{3.14}$$

where A, B and C are constants defined by

$$A = \psi_4|_{\eta=1.7} = \frac{2 - 2\cosh(1.7) + 1.7\sinh(1.7)}{\cosh(1.7) - 1} = 0.46, \tag{3.15}$$

$$B = \psi_5|_{\eta=1.7} = -\frac{1}{2}\frac{4 - 4\cosh(1.7) + 5.1\sinh(1.7) - \sinh^2(1.7)}{\cosh(1.7) - 1} = 0.22, \tag{3.16}$$

and

$$C = \psi_6|_{\eta=1.7} = -\frac{\sinh(1.7)}{\cosh(1.7) - 1} = 1.45, \tag{3.17}$$

respectively. For $S(\tau_c)$ to be timelike at $\eta = 1.7$, $\mathcal{R} < 1$ in equation (3.14) leads to

$$\sqrt{\frac{1+f}{f}} > \left|\left(A\frac{M'}{a'f^{3/2}} + B\frac{Mf'}{a'f^{5/2}}\right) - C\right|. \tag{3.18}$$

and since the scale time $\tilde{T}$ is defined as $M/|f|^{3/2}$, equation (3.18) can be rewritten as

$$\sqrt{\frac{1+f}{f}} > \left|\frac{\tilde{T}}{a'}\left(A\frac{M'}{M} + B\frac{f'}{f}\right) - C\right|. \tag{3.19}$$

Where it is true, $S(\tau_c)$ will be timelike, otherwise spacelike.

- At late times ($\eta \to \infty$), equation (3.6) reduces to

$$\mathcal{R} \approx \frac{1}{|a'|\sqrt{1+f}}\left|\frac{M'}{f}\eta + \frac{Mf'}{f^2}\frac{e^\eta}{4} + (-a')\sqrt{f}\right|. \tag{3.20}$$

If $a' \neq 0$, $S(\tau_c)$ becomes timelike only if $M' = f' = 0$. Thus, equation (3.20) reduces to

$$\mathcal{R} = \sqrt{\frac{f}{1+f}} \leq 1. \tag{3.21}$$

If $a' = 0$, equation (3.20) goes to infinity because the denominator is equal to zero and the $S(\tau_c)$ surfaces become spacelike everywhere. Generally, $S(\tau_c)$ is timelike at late times only if $M' = f' = 0$, otherwise it is spacelike.

3.2.2 Elliptic Regions

It was indicated in §2.6 that, at early times ($\eta \to 0$), $\psi_1 \approx (\eta^2/6)$, $\psi_2 \approx (\eta^4/40)$ and $\psi_3 \approx (2/\eta)$, whereas at late times ($\eta = 2\pi - \delta, \delta \to 0$), $\psi_1 \approx (4\pi/\delta)$, $\psi_2 \approx (6\pi/\delta)$ and $\psi_3 \approx (-2/\delta)$. Let us next investigate the ratio $\mathcal{R}$ of equation (3.8) for different time domains.

- At early times ($\eta \to 0$), equations (3.7) and (3.8) reduce to

$$\left.\frac{dt}{dr}\right|_n = \pm\frac{1}{\sqrt{1+f}}\left(\frac{M'}{(-f)}\frac{\eta^2}{6} + \frac{Mf'}{f^2}\frac{\eta^4}{40} + (-a')\sqrt{(-f)}\frac{2}{\eta}\right) \approx \pm\frac{2(-a')}{\eta}\sqrt{\frac{(-f)}{1+f}}, \tag{3.22}$$

  and

$$\mathcal{R} = \frac{1}{|a'|\sqrt{1+f}}\left|\frac{M'}{(-f)}\frac{\eta^2}{6} + \frac{Mf'}{f^2}\frac{\eta^4}{40} + (-a')\sqrt{(-f)}\frac{2}{\eta}\right| \approx \frac{2}{\eta}\sqrt{\frac{(-f)}{1+f}}, \tag{3.23}$$

  respectively, assuming $a' \neq 0$. Equation (3.23) goes to infinity where $a' \neq 0$ because ψ_3 diverges, which means that $S(\tau_c)$ becomes spacelike. If $a = 0$, equation (3.23) goes directly to infinity because the denominator is equal to zero, and $S(\tau_c)$ is spacelike in this case too. Generally, $S(\tau_c)$ is spacelike everywhere at early times.

- At intermediate times, which we choose to mean maximum expansion, $\eta = \pi$, equations (3.7) and (3.8) reduce to

$$\left.\frac{dt}{dr}\right|_n = \pm\frac{-2M'f + 2Mf'}{f^2\sqrt{1+f}}, \tag{3.24}$$

  and

$$\mathcal{R} = \frac{|-2M'f + 2Mf'|}{|a'|f^2\sqrt{1+f}} = \frac{1}{|a'|\sqrt{1+f}}\left|\frac{-2M'}{f} + \frac{2Mf'}{f^2}\right|, \tag{3.25}$$

  respectively, because $\psi_1 = -2$, $\psi_2 = 2$ and $\psi_3 = 0$. Since the scale length is defined as

$$\tilde{R} = \frac{M}{|f|}, \tag{3.26}$$

  where its derivative is given by

$$\tilde{R}' = \frac{M'}{|f|} + \frac{Mf'}{f^2}. \tag{3.27}$$

Equation (3.25) can be written in terms of equation (3.27) as

$$\mathcal{R} = \frac{2|\tilde{R}'|}{|a'|\sqrt{1+f}}. \tag{3.28}$$

Applying the timelike condition $\mathcal{R} < 1$, equation (3.28) gives

$$|a'| > \frac{|\tilde{R}'|}{\sqrt{1+f}}. \tag{3.29}$$

and if not true, $S(\tau_c)$ will be spacelike at maximum expansion.

- At late times ($\eta = 2\pi - \delta, \delta \to 0$), equations (3.7) and (3.8) reduce to

$$\left.\frac{dt}{dr}\right|_n = \pm\frac{1}{\sqrt{1+f}}\left(\frac{M'}{(-f)}\frac{4\pi}{\delta} + \frac{Mf'}{f^2}\frac{6\pi}{\delta} + (-a')\sqrt{(-f)}\left(\frac{-2}{\delta}\right)\right), \tag{3.30}$$

and

$$\begin{aligned}
\mathcal{R} &= \frac{1}{|a'|\sqrt{1+f}}\left|\frac{M'}{(-f)}\frac{4\pi}{\delta} + \frac{Mf'}{f^2}\frac{6\pi}{\delta} + (-a')\sqrt{(-f)}\left(\frac{-2}{\delta}\right)\right|, \\
&= \frac{1}{|a'|\sqrt{1+f}}\left|\frac{4\pi\tilde{T}}{\delta}\left(\frac{M'}{M} - \frac{3f'}{2f}\right)\sqrt{(-f)} + \sqrt{(-f)}\frac{2a'}{\delta}\right|, \\
&= \frac{1}{|a'|\sqrt{1+f}}\left|\frac{2\sqrt{(-f)}}{\delta}(2\pi\tilde{T}' + a')\right| = \frac{2\left|2\pi\tilde{T}' + a'\right|}{|a'|\delta}\sqrt{\frac{(-f)}{1+f}},
\end{aligned} \tag{3.31}$$

respectively if $a' \neq 0$. It is clear that $\mathcal{R} = 0$ only when $2\pi\tilde{T}' + a' = 0$ and $a' \neq 0$, which makes $S(\tau_c)$ a timelike surface, and otherwise $\mathcal{R}$ is divergent. If $a' = 0$, equation (3.31) goes to infinity because the denominator is equal to zero and thus $S(\tau_c)$ is spacelike. We find that $S(\tau_c)$ becomes timelike near the big crunch only if the crunch time is constant and the big bang time is not, $2\pi\tilde{T}' + a' = 0$ and $a' \neq 0$.

Finally, we can summarize these results in table 3.1.

	At early time	At intermediate time	At late time
Hyperbolic case	• If $a' \neq 0$, $S(\tau_c)$ is spacelike. • If $a' = 0$, $S(\tau_c)$ is spacelike.	• $S(\tau_c)$ becomes timelike only if $$\sqrt{\frac{1+f}{f}} > \left\lvert \frac{\tilde{T}}{a'}\left(A\frac{M'}{M} + B\frac{f'}{f}\right) - C \right\rvert$$	• If $a' \neq 0$, $S(\tau_c)$ is timelike only if $M' = f' = 0$. • If $a' = 0$, $S(\tau_c)$ is spacelike.
	• Generally, $S(\tau_c)$ is spacelike everywhere at early time.	• Otherwise, $S(\tau_c)$ is spacelike.	• Generally, $S(\tau_c)$ is spacelike if conditions $M' = f' = 0$ and $a' \neq 0$ do not hold.
Elliptic case	• If $a' \neq 0$, $S(\tau_c)$ is spacelike • If $a' = 0$, $S(\tau_c)$ is spacelike	• $S(\tau_c)$ becomes timelike only if $$\lvert a' \rvert > \frac{\lvert \tilde{R}' \rvert}{\sqrt{1+f}}$$	• $S(\tau_c)$ is timelike only if $a' \neq 0$ and $$2\pi\tilde{T}' + a' = 0$$
	• Generally, $S(\tau_c)$ is spacelike everywhere at early time.	• Otherwise, $S(\tau_c)$ is spacelike.	• Otherwise, $S(\tau_c)$ is spacelike.

TABLE 3.1: Summary of the Conditions for $S(\tau_c)$ to be Spacelike or Timelike at Early, Middle and Late Times

Chapter 4

Explicit Models

We considered several different time regimes of Lemaître-Tolman models in chapter 3, and derived the necessary and sufficient conditions for the constant Ricci time surfaces, $S(\tau_c)$, to be timelike or spacelike. The main purpose of this chapter is to investigate numerically the detailed behaviour of these surfaces in a range of different explicit LT models, including elliptic and hyperbolic cases. We will create various models with different behaviors, which allow us to examine these conditions, and visualize the character of $S(\tau_c)$ in (t, r) plots. We also check if the regions of timelike $S(\tau_c)$ occur inside or outside the apparent horizons.

4.1 Numerical Calculations

We have developed a numerical code that takes the definitions of the LT arbitrary functions and calculates $dt/dr|_n$, $dt/dr|_\tau$ and $\mathcal{R}$, as detailed in chapter 3. The resulting data is plotted against r and t as a pair of surfaces of different colours, whose heights above the (t, r) plane are the slopes $dt/dr|_n$ and $dt/dr|_\tau$. In fact we experimented with several plotting formats, and we found that this one shows most clearly where $S(\tau_c)$ changes between spacelike and timelike. In order to check that our model choices were reasonable and free of irregularities, the code also produces plots of $M(r)$, $f(r)$, $a(r)$ and $\tilde{T}(r)$, as well as the functions that indicate a shell crossing if they have the wrong sign, $M'(r)$, $f'(r)$, $a'(r)$ and $2\pi\tilde{T}'(r) + a'(r)$. Out of these last 4 functions, the first 3 are relevant to hyperbolic regions, and functions 1, 3 and 4 are relevant to elliptic models (see table 2.1).

The actual code must allow for a few practical numerical issues.

- The slope $dt/dr|_n$ diverges near the bang and the crunch, and this must be chopped by not plotting certain η values.

- In elliptic regions, if the big crunch occurs within the time range plotted, the two surfaces must be terminated just before the crunch.

- The apparent horizon (AH) is the locus along a radial light ray where R changes from increasing to decreasing. Using equations (3.3) and (2.4) this gives

$$\left.\frac{dR}{dr}\right|_n = 0 = \dot{R}\left.\frac{dt}{dr}\right|_n + R' = \dot{R}\left(\frac{\pm R'}{\sqrt{1+f}}\right) + R' = \left(\frac{\mp\sqrt{2M/R+f}}{\pm\sqrt{1+f}} + 1\right)R', \tag{4.1}$$

  which leads to

$$R_{AH} = 2M. \tag{4.2}$$

  By equations (2.7) and (2.9)

$$\cosh\eta_{AH} = 2f+1, \qquad t_{AH} = a + (\sinh\eta_{AH} - \eta_{AH})M/f^{3/2} \tag{4.3}$$

$$\cos(\eta_{AH}) = 2f+1, \qquad t_{AH} = a + (\eta_{AH} - \sin\eta_{AH})M/(-f)^{3/2} \tag{4.4}$$

  for hyperbolic and elliptic cases, respectively. Since we are using η in the evolution calcuations, this is the easiest way to calculate the AH locus on each constant r worldline. The apparent horizon is a locus in the (t, r) plane. In fact there are two AHs in elliptic region. For clarity, the AH curves are plotted on the null slope surfaces, i.e. at "height" $dt/dr|_n$ on the plot, otherwise they would be hidden.

- As noted above, the origin and spatial extrema in R generate undefined zero-over-zero values unless their limits are evaluated properly. Therefore, the various arbitrary funtion combinations appearing in equations (3.5) to (3.8), such as $Mf'/f^2/\sqrt{1+f}/a'$ and $\sqrt{f/(1+f)}$, must be re-evaluated analytically for each choice of M, f and a. Each of these function combinations must be written into the code explicitly.

The general algorithm is as follows.

1. Define the ranges of r and η, where r changes from 0 to 0.9, while η extends from 0 to 7.2.

2. Define the arbitrary functions M, f, a and their derivatives M', f', a' as functions of r. Moreover, define a number of other ratios like M/f and $M/f^{3/2}$.

3. Rescale η to be $\tilde{\eta}$ given by equation (2.49) in order to avoid vastly different timescales in the same plot. and handle near-parabolic regions without trouble.

4. In terms of $\tilde{\eta}$, calculate ψ_1, ψ_2 and ψ_3 for elliptic regions, as given by equations (2.11), (2.12) and (2.13), respectively. Similarly, evaluate ψ_4, ψ_5 and ψ_6 for hyperbolic regions, as given by equations (2.15), (2.16) and (2.17), respectively. Redefine these functions as series approximations when η approaches zero and 2π.

5. Depending on the value of $\tilde{\eta}$, calculate R, t, $dt/dr|_n$, $dt/dr|_\tau$ and $\mathcal{R}$ for the whole range, using the appropriate elliptic or hyperbolic expressions.

6. Plot the two slopes as intersecting 2-d surfaces in a 3-d plot.[1]

7. Evaluate the apparent horizon locus, and draw it as a black line on the $dt/dr|_n$ surface.

8. Plot the LT arbitrary functions and the no shell crossing condition functions.

4.2 Hyperbolic Models

4.2.1 Model 1

The arbitrary functions are

$$M = M_0(r^3 + M_1 r^4 + M_2 r^5), \tag{4.5}$$

$$f = -k(r^2 + f_1 r^3 + f_2 r^4), \tag{4.6}$$

$$a = a_0 + a_1 r + a_2 r^2 + a_3 r^3, \tag{4.7}$$

where $M_0 = 1$, $M_1 = -3$, $M_2 = 2.4$, $k = -1$, $f_1 = -2.67$, $f_2 = 2$, $a_0 = 5$, $a_1 = -200$, $a_2 = 0.5$ and $a_3 = 0.9$. This is the first set of coefficients, we will use with model (1). This is an inhomogeneous model with non-zero density everywhere, so it is a "cosmology". These functions were specifically selected so that both M and f have zero gradient at the same r value, but never have a negative gradient. Therefore we have a worldline (r value) which satifies the condition $M' = f' = 0$, as shown in figure 4.1a, which should make $S(\tau_c)$ timelike at late times, and the neighbouring worldlines are very close to that condition.

Figure 4.1a shows the behavior of the arbitrary functions M, f and a which represent an inhomogeneous hyperbolic model where $f > 0$. Functions M and f increase smoothly while a decreases rapidly with increasing r. Scale time $\tilde{T}$ is not necessarily increasing, but has a zero gradient at the same point as functions M and f. Figure 4.1b shows the conditions for no shell crossings are satisfied, because $M' \geq 0$, $f' \geq 0$ and $a' \leq 0$ clearly hold. We ignore the fourth condition $2\pi\tilde{T}' + a' \geq 0$ because we deal only with hyperbolic model where $f > 0$.

[1] Several other plots, such as $\mathcal{R}$ against t and R, are plotted but not used here.

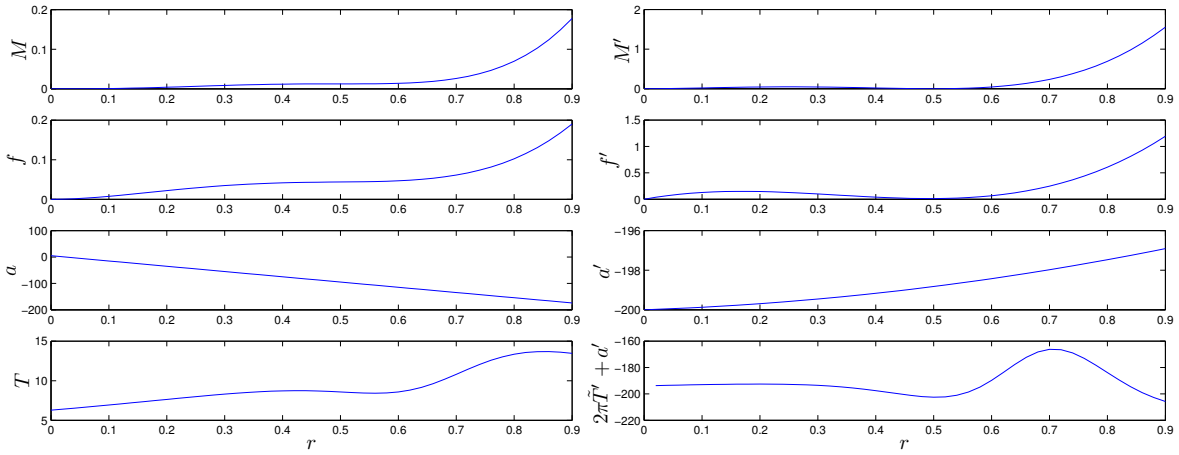

(A) The behavior of M, f, a and $\tilde{T}$

(B) Conditions for no shell crossings.

FIGURE 4.1: Hyperbolic model (1) using the first set of coefficients: The behavior of the arbitrary functions and the no shell crossing conditions.

Figure 4.2 illustrates the relation between the {constant τ} surfaces $S(\tau_c)$ and the radial null surfaces for each worldline and a sufficiently large range of the evolution. The red and blue surfaces represent the slopes of $S(\tau_c)$ and the null surfaces, respectively. The black line shows the apparent horizon, which allows us to indicate whether the timelike $S(\tau_c)$ regions occur inside (at smaller R) or outside (at larger R) the AH. Our hyperbolic model is always expanding, so smaller R occurs to the past of the black line. For each world line r, the behavior of the $S(\tau_c)$ changes depending on the arbitrary functions. To illustrate, let us examine the nature of these surfaces in three regions. The first region starts from the origin to $r = 0.3$, the second region extends from 0.3 to 0.7 and the third region lies between 0.7 and 0.9.

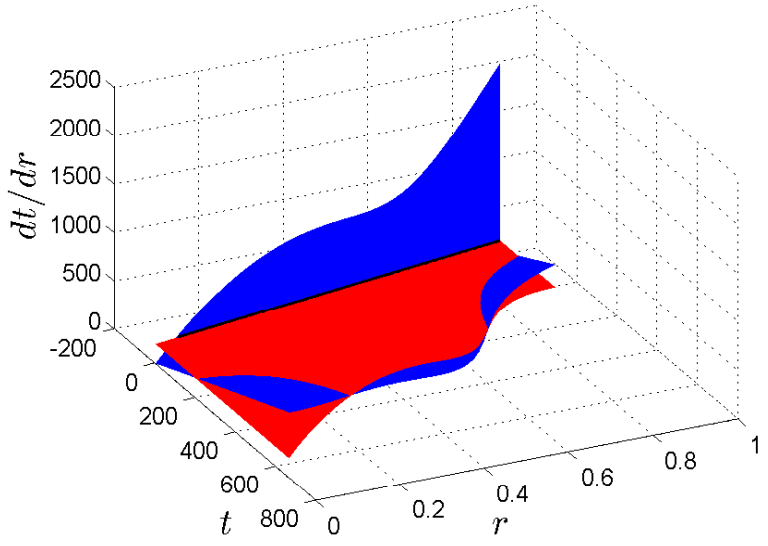

FIGURE 4.2: Hyperbolic model (1) using the first set of coefficients: The slopes of the $S(\tau_c)$ and radial null surfaces, $dt/dr|_\tau$ and $dt/dr|n$, shown in red and blue respectively, are plotted against t and r. Where the red surface is above the blue one, $S(\tau_c)$ is timelike. The black line represents the apparent horizon, and the big bang is where the blue surface rises at the back.

For the first region ($0 < r < 0.3$), the $S(\tau_c)$ becomes spacelike at early and late times. For intermediate times, the slope of $S(\tau_c)$ changes to timelike for at least part of the evolution, as shown in figure 4.1b. We noticed that the size (duration) of the timelike region, at the intermediate times, can be increased by increasing $(-a')$. Conversely, the size of the timelike region is decreased by decreasing $(-a')$, and it shrinks towards the bang. This is discussed further below. For the second region ($0.3 < r < 0.7$), the $S(\tau_c)$ are spacelike at early times. At the intermediate times, they become timelike and remain timelike for the rest of the plotted evolution. It is clear that the r value for which $M' = f' = 0$, $r = 0.5$, as shown in figure 4.2, is at the middle of this range. The third region ($0.7 < r < 0.9$) has the same behavior as the first region ($0 < r < 0.3$). The black line indicates that the timelike region is located outside the apparent horizon, at larger R. This model confirms that $S(\tau_c)$ is spacelike everwhere for early times, but at late times $S(\tau_c)$ can have a different behavior, being either spacelike or timelike, depending on whether M' and f' are zero.

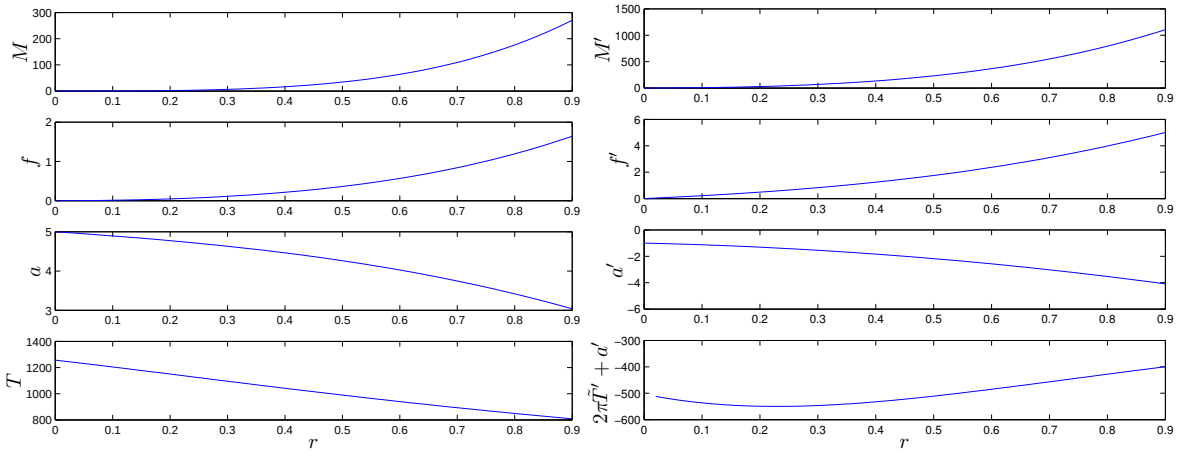

(A) The behavior of M, f, a and $\tilde{T}$ (B) Conditions for no shell crossings.

FIGURE 4.3: Hyperbolic model (1) using the second set of coefficients: The behavior of the arbitrary functions and the no shell crossing conditions.

Now, by changing the coefficients of the arbitrary functions in equations (4.5)-(4.7), we can produce a model for which $S(\tau_c)$ is spacelike area everywhere. For instance, taking $M_0 = 200$, $M_1 = 0.5$, $M_2 = 0.5$, $k = -1$, $f_1 = 0.6$, $f_2 = 0.6$, $a_0 = 5$, $a_1 = -1$, $a_2 = -0.5$ and $a_3 = -0.9$ as the second set of coefficients, the behavior of the functions is slightly changed, as shown in figure 4.3a. Functions M and f increase rapidly while a deceases smoothly as r increases. The scale time $\tilde{T}$ decreases with increasing r. Figure 4.3b shows the conditions for no shell crossings are satisfied since $M' \geq 0$, $f' \geq 0$ and $a' \leq 0$. The blue $dt/dr|_n$ surface in figure 4.4 is everywhere above the red $dt/dr|\tau$ surface, showing that $S(\tau_c)$ is always spacelike for each world line, because $M' > 0$ and $f' > 0$ as shown in figure 4.3a. The bold black line visualizes the apparent horizon.

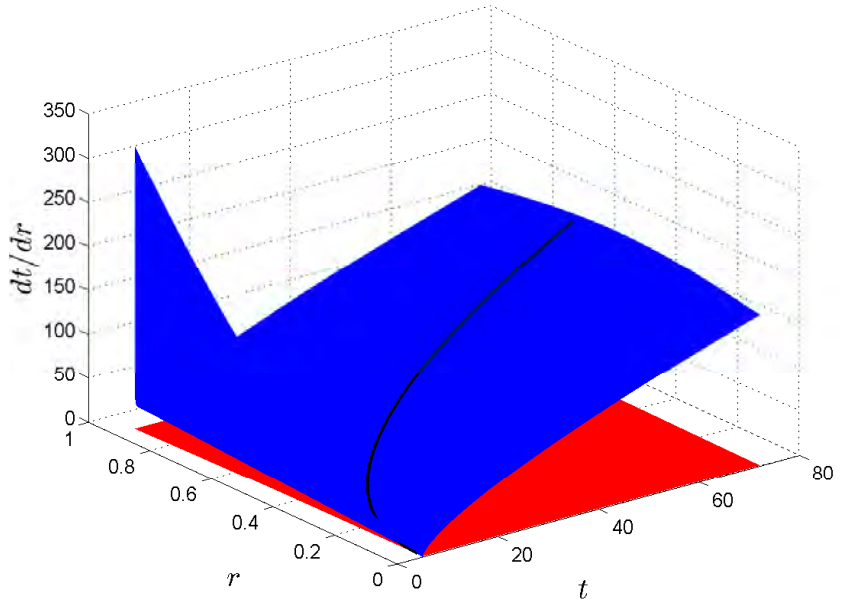

FIGURE 4.4: Hyperbolic model (1) using the second set of coefficients: The slopes of the $S(\tau_c)$ and radial null surfaces, showing $S(\tau_c)$ is spacelike everywhere.

By using a third set of arbitrary functions and varying just one of them, we can investigate the nature of the intermediate time. Choosing $M_0 = 1$, $M_1 = -2$, $M_2 = 1.4$, $k = -1$, $f_1 = -1.65$, $f_2 = 1$, $a_0 = 0$, $a_1 = -200$, $a_2 = 0.1$ and $a_3 = 0.1$, the behavior of the functions and the conditions for no shell crossings are represented in Figures 4.5a and 4.5b, respectively. The coefficient a_1 will be varied.

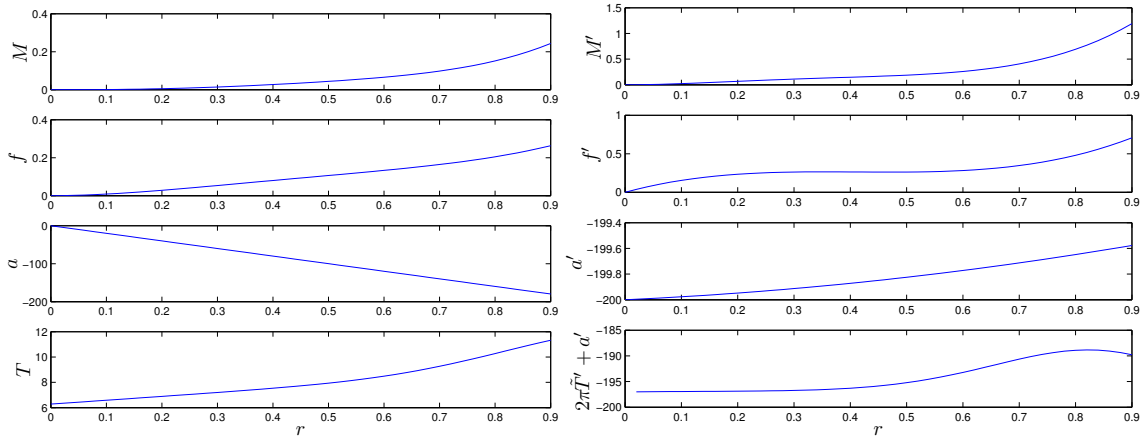

(A) The behavior of M, f, a and $\tilde{T}$

(B) Conditions for no shell crossings.

FIGURE 4.5: Hyperbolic model (1) using the third set of coefficients and $a_1 = -200$: The behavior of the arbitrary functions and the no shell crossing conditions.

With $a_1 = -200$, which creates a moderately large value of $(-a')$, the $S(\tau_c)$ are spacelike for all r, at both early and late times, but they still becomes timelike at intermediate times. This is shown in figure 4.6. If $(-a')$ is made very large by changing $a_1 = -2000$, the $S(\tau_c)$ are of course spacelike at the earliest times, but become timelike just after the AH, and remain timelike up to very late times on all worldlines, as shown in figure 4.7a. This timelike

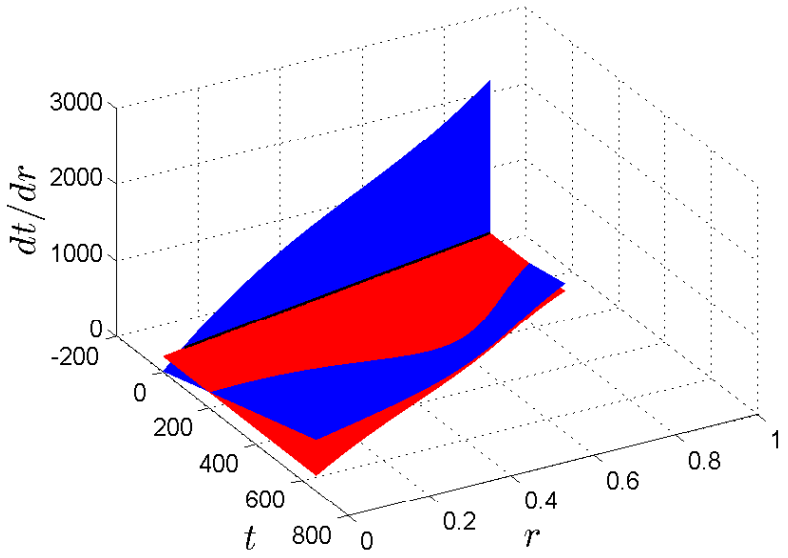

FIGURE 4.6: Hyperbolic model (1) using the third set of coefficients and $a_1 = -200$: The slopes of the $S(\tau_c)$ and null surfaces are shown and here $S(\tau_c)$ is timelike only at intermediate times.

region is at "intermediate times" since $M' > 0$ and $f' > 0$, so the $S(\tau_c)$ must eventually become spacelike again. If $(-a')$ is made small by changing $a_1 = -0.2$, the $S(\tau_c)$ now become spacelike everywhere at all times, as shown in figure 4.7c. In other words, by decreasing $(-a')$, the extent of the timelike region can be decreased and made to vanish for small enough $(-a')$. Moreover, the timelike region shrinks towards the origin as $(-a')$ is decreased.

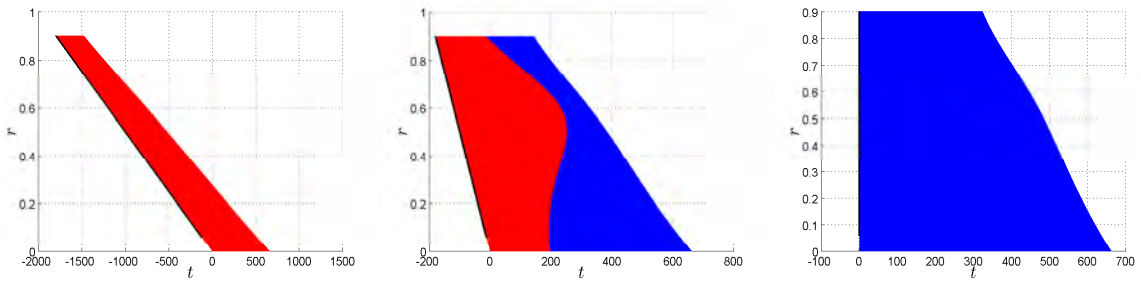

(A) a_1 = -2000 (B) a_1 = -200 (C) a_1 = -0.2

FIGURE 4.7: Hyperbolic model (1) using the third set of coefficients and 3 different a_1 values: This is a view looking straight "down", so the "heights" dt/dr are not seen. The sizes of the red regions show the sizes of the regions of timelike $S(\tau_c)$. The black line is the apparent horizon.

4.2.2 Model 2

The arbitrary functions are

$$M = M_0 \exp(1 + M_1 r), \tag{4.8}$$

$$f = -k \exp(1 + f_1 r), \tag{4.9}$$

$$a = a_0 \exp(1 + a_1 r), \tag{4.10}$$

where $M_0 = 2$, $M_1 = 0.01$, $k = -1$, $f_1 = 0.1$, $a_0 = -0.01$ and $a_1 = 5$. As shown in figure 4.8a, functions M and f increase while a and $\tilde{T}$ decrease as r increases. This is a hyperbolic model with an unusual topology, because the "origin" is asymptotically far away at $r = -\infty$. However, figure 4.8b shows the conditions for no shell crossings are satisfied.

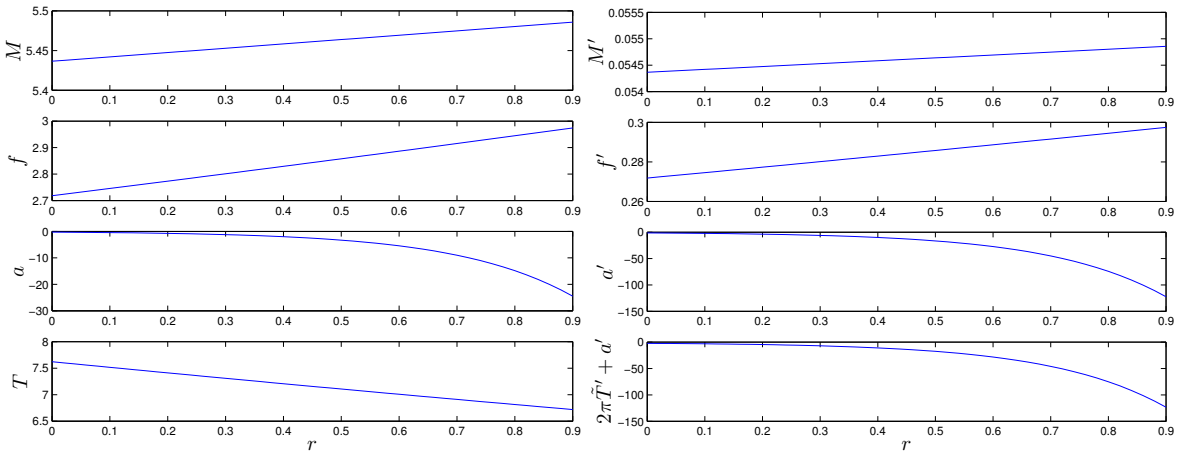

(A) The behavior of M, f, a and $\tilde{T}$

(B) Conditions for no shell crossings.

FIGURE 4.8: Hyperbolic model (2): The behavior of the arbitrary functions and the no shell crossing conditions.

At early times, $S(\tau_c)$ is spacelike everywhere, but $S(\tau_c)$ becomes timelike at intermediate times for a specific region depending on the arbitrary functions. As before, the size of the timelike region depends strongly on $(-a')$, decreasing with smaller $(-a')$ and increasing with larger $(-a')$. Note that the timelike region occurs outside the AH as explained before. At late times, the $S(\tau_c)$ surfaces eventually become spacelike again.

Generally, for hyperbolic models 1 and 2, the surfaces $S(\tau_c)$ are spacelike everywhere at early times, and timelike regions seem common at intermediate times unless a' is very small. However the $S(\tau_c)$ are nearly always spacelike in the late time limit, except for the rather special case that $M' = f' = 0$ on certain worldlines. For worldlines that are very close to this condition, the timelike character of the $S(\tau_c)$ can remain until very late times. In the cases looked at, the timelike region always occurs outside the horizon, but often very close to it.

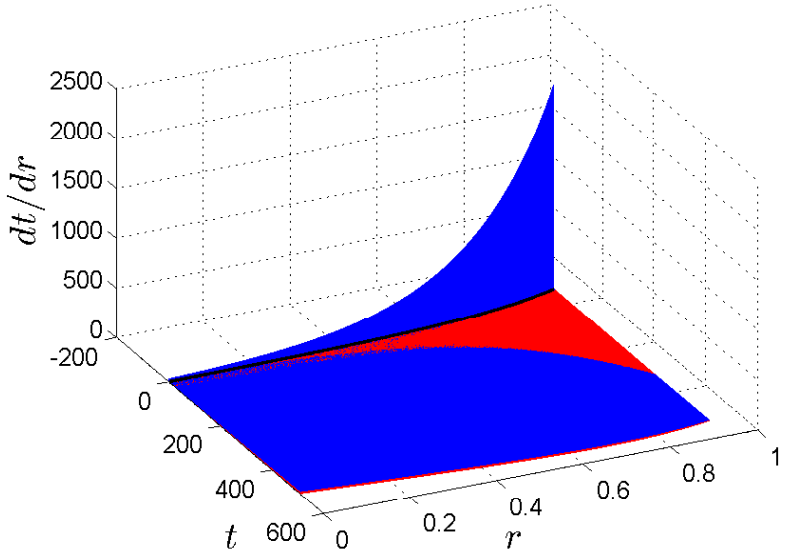

FIGURE 4.9: Hyperbolic model (2): The slopes of the $S(\tau_c)$ and null surfaces are indicated by the heights of the red and blue surfaces in this plot, and $S(\tau_c)$ is timelike where the red surface is higher.

4.3 Elliptic Models

4.3.1 Model 1

The chosen arbitrary functions are

$$M = M_0(r^3 + M_1 r^4 + M_2 r^5), \tag{4.11}$$

$$f = -k(r^2 + f_1 r^3 + f_2 r^4), \tag{4.12}$$

$$a = a_0 + a_1 r + a_2 r^2 + a_3 r^3, \tag{4.13}$$

where $M_0 = 1$, $M_1 = 0$, $M_2 = 2.4$, $k = 1$, $f_1 = -0.67$, $f_2 = 0$, $a_0 = 5$, $a_1 = -5$, $a_2 = 0.5$ and $a_3 = 0.9$. This is the first coefficient set. This function set represents an inhomogeneous elliptic cosmology (since $\rho > 0$), with $f < 0$ as shown in figure 4.10a. Functions M and $\tilde{T}$ increase while f and a decrease with increasing r. Although these functions would not work globally, they are entirely valid for the range of r calculated. Figure 4.10b illustrates the no shell crossing conditions, and here we verify that $M' \geq 0$, $a' \leq 0$ and $2\pi\tilde{T}' + a' > 0$ hold in the r range under consideration. For elliptic models the f' plot is not relevant.

Figure 4.11 illustrates the relationship between the $S(\tau_c)$ and the null surfaces, whose slopes are represented by the heights of the red and blue surfaces respectively, in the 3-d plot. The bold black lines show the loci of the apparent horizons. At early and late times, the $S(\tau_c)$ surfaces are spacelike everywhere. $S(\tau_c)$ becomes timelike at the intermediate times, for a

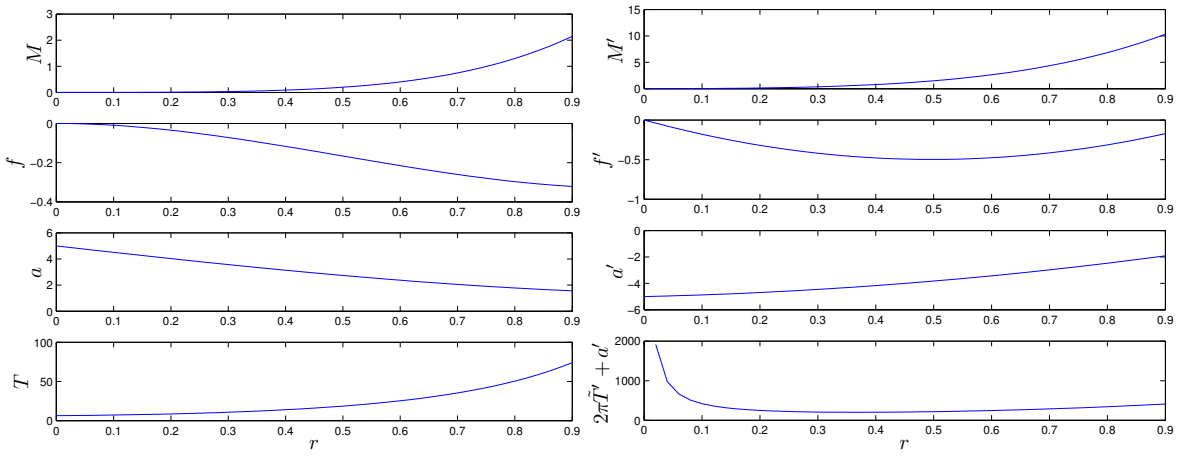

(A) The behavior of M, f, a and $\tilde{T}$ (B) Conditions for no shell crossings.

FIGURE 4.10: Elliptic model (1) with the first coefficient set: The behavior of the LT arbitrary functions and the no shell crossing conditions.

range of worldlines ($0 < r < 0.3$) and remains spacelike through the whole evolution for the rest. The size of the timelike region can once again be developed by altering ($-a'$), specifically the timelike region is expanded by increasing ($-a'$) and contracted by decreasing ($-a'$), with the region near the origin disappearing last.

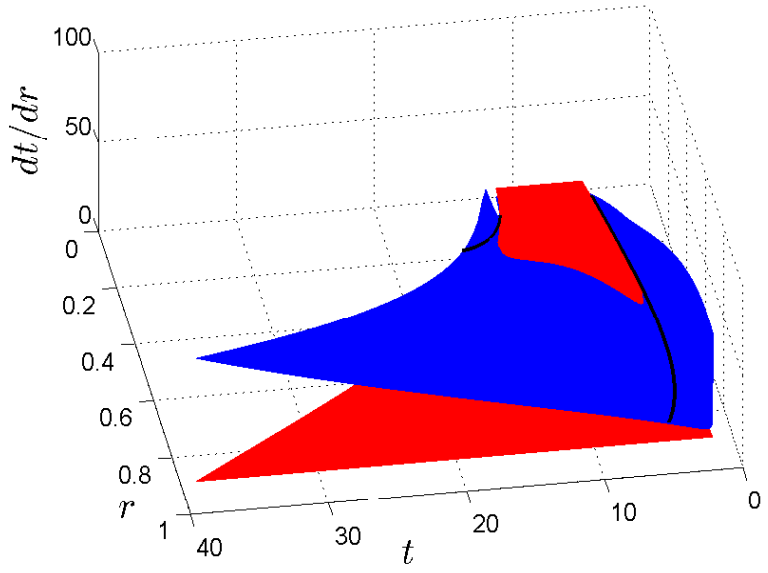

FIGURE 4.11: Elliptic model (1) with the first coefficient set: The relationship between the $S(\tau_c)$ and null surfaces, where the heights of the red and blue colours represent the slopes of the $S(\tau_c)$ and null surfaces, respectively. The black lines represent the past and future apparent horizons.

The region of timelike $S(\tau_c)$ lies between the two AHs (though outside them, i.e. at larger R), but lies very close to them for quite a range of r. Now let us investigate how the size of the timelike region is affected by adjusting the crunch time. We will keep the scale time $\tilde{T}$ unchanged, but adjust a to make the crunch time constant. We therefore use the same $M(r)$

and $f(r)$ as in equations (4.11)-(4.12), but change a to be

$$a = -2\pi\tilde{T} = -2\pi\frac{M}{f^{3/2}}, \tag{4.14}$$

The coefficients are changed to $M_0 = 1$, $M_1 = 0.1$, $M_2 = 0.1$, $k = 1$, $f_1 = -0.67$ and $f_2 = 0$, which is the second coefficient set. Figure 4.12a indicates the behavior of the arbitrary functions for this case; $M(r)$ and $f(r)$ are only slightly different from previously. Figure 4.12b verifies that $M' \geq 0$, $a' \leq 0$ and $2\pi\tilde{T}' + a' = 0$, thereby satisfying the no shell crossing conditions.

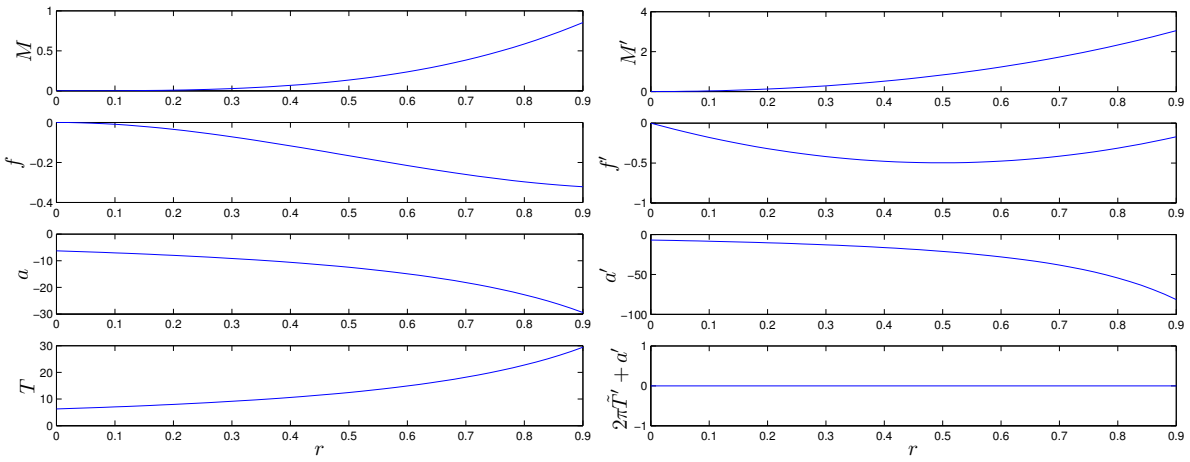

(A) The behavior of M, f, a and $\tilde{T}$

(B) Conditions for no shell crossings.

FIGURE 4.12: Elliptic model (1) with the second coefficient set: The behavior of the arbitrary functions and the no shell crossing conditions.

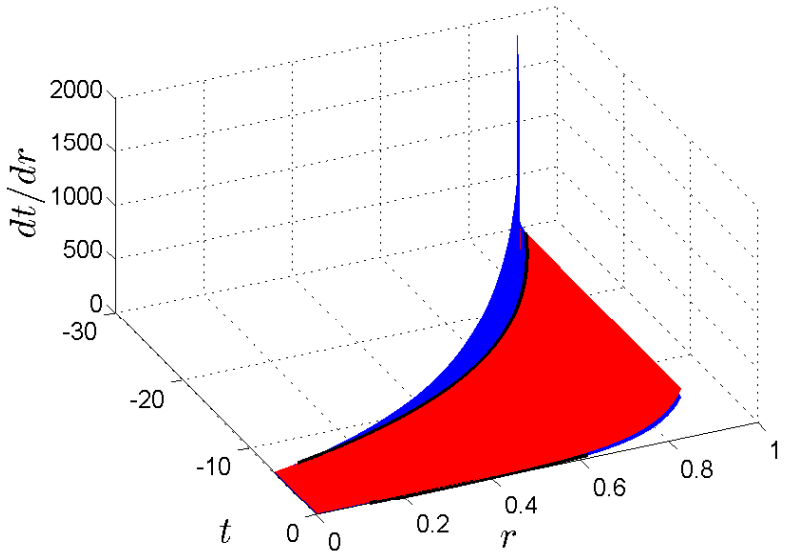

FIGURE 4.13: Elliptic model (1) with the second coefficient set: The relationship between the $S(\tau_c)$ and null surfaces. Here the $S(\tau_c)$ surfaces are spacelike at early times, but timelike at intermediate and late times. The crunch is not included in the plotted range for the larger r worldlines.

At early times, the $S(\tau_c)$ surfaces are spacelike everywhere. At the intermediate and late times they become timelike for a constant crunch time, as shown in figure 4.13.

This situation can be changed if a is made a different multiple of lifetime $\tilde{T}$. For instance, if $a = -0.9(2\pi\tilde{T})$, the $S(\tau_c)$ are spacelike at early times, and stay timelike through intermediate up to quite late times. If $a = -0.2(2\pi\tilde{T})$, the $S(\tau_c)$ become timelike at intermediate times and return to spacelike quite soon thereafter, as shown in figure 4.14. In this case, we find two discrete timelike regions. One of these regions is close to the bang while the other is close to crunch and the origin. If $a = -0.01(2\pi\tilde{T})$, the $S(\tau_c)$ become spacelike everywhere. We notice that the size of the timelike region in intermediate times, decreases for small $(-a')$ and increases for large $(-a')$. Furthermore, the timelike region or regions are always outside the apparent horizons (the black lines), though often very close to them.

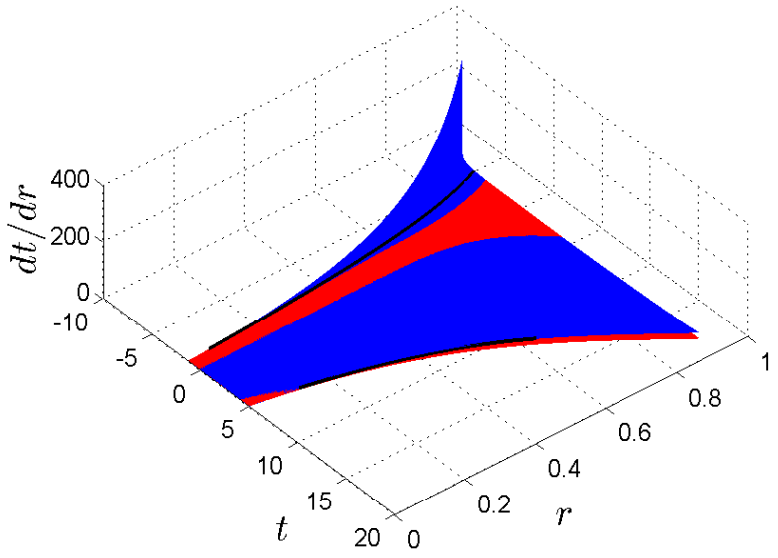

FIGURE 4.14: Elliptic model (1) with the second coefficient set and $a = -0.2(2\pi\tilde{T})$: The character of the $S(\tau_c)$ and null surfaces, showing the $S(\tau_c)$ are timelike only at intermediate times. The plotted evolution range does not reach the crunch at larger r values.

Figure 4.15 shows the variation of the timelike region size as the strength of the bang time variation, relative to the lifetime, is decreased; $a = -\alpha(2\pi\tilde{T})$ with α varying. The value $\alpha = 1$ gives a constant crunch time. Generally in this model, the timelike region extends to late times (i.e. the crunch) only if the crunch time is constant. The size of the timelike region can be increased by increasing $(-a')$ and vice versa, but it is confined to be outside the AHs, though often lying very close to them.

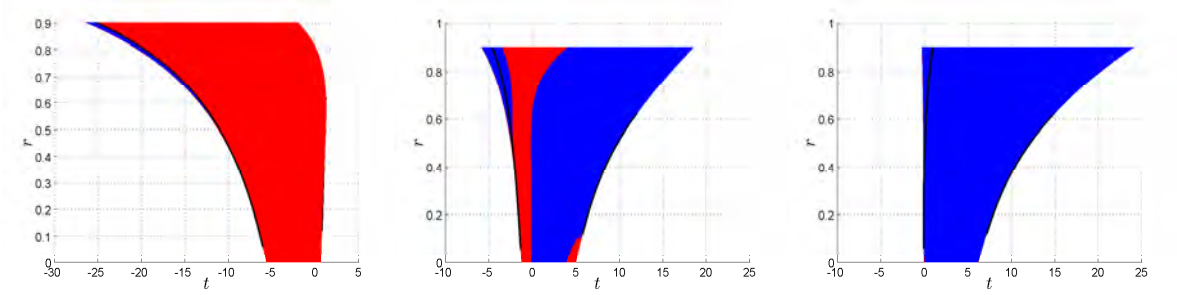

(A) $a = -0.9(2\pi\tilde{T})$ (B) $a = -0.2(2\pi\tilde{T})$ (C) $a = -0.01(2\pi\tilde{T})$

FIGURE 4.15: Elliptic model (1) with the second coefficient set and different bang times: The extent of the timelike $S(\tau_c)$ region is strongly affected by this variation.

4.3.2 Model 2

For this model the arbitrary functions are

$$M = M_0 + M_1 \exp(r^2/M_2), \tag{4.15}$$

$$f = -k \exp(r^2/f_2), \tag{4.16}$$

$$a = a_2 r^2, \tag{4.17}$$

where $M_0 = 2$, $M_1 = 1$, $M_2 = 0.1$, $k = 1$, $f_2 = 0.1$ and $a_2 = -1$. Plots of these functions and of the no shell crossing conditions can be found in figures 4.16a and 4.16b, respectively.

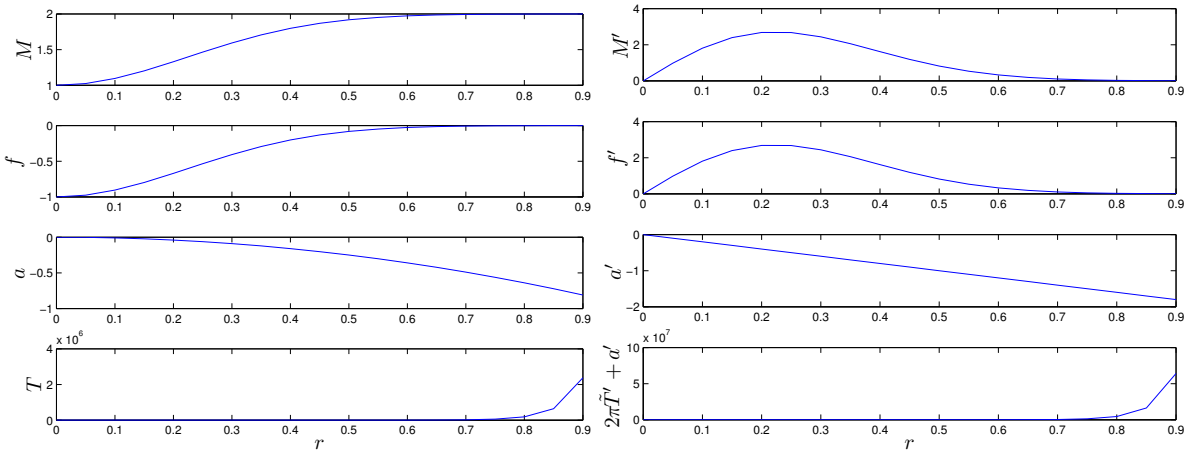

(A) The behavior of M, f, a and $\tilde{T}$ (B) The no shell crossing conditions

FIGURE 4.16: Elliptic model (2): The behavior of the LT arbitrary functions that describe a non-vacuum black hole and the associated no shell crossing conditions.

This choice of functions gives an elliptic model, $f < 0$, which represents a non-vacuum black hole, with matter flowing out of the past singularity (or bang) and into the future singularity (or crunch). The $S(\tau_c)$ surfaces become timelike at intermediate times, while at early and late times the $S(\tau_c)$ are spacelike everywhere. We notice that the timelike region decreases in size for small $(-a')$ and increases for large $(-a')$.

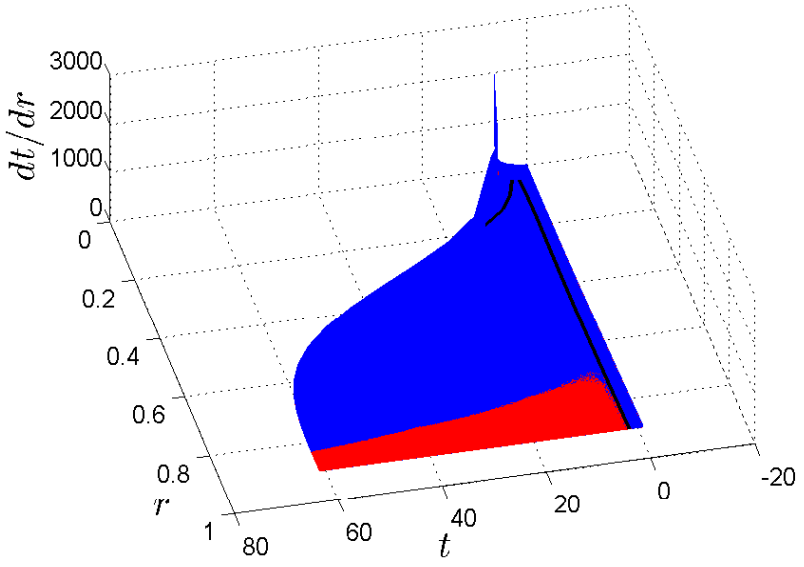

FIGURE 4.17: Elliptic model (2): The character of the $S(\tau_c)$ and null surfaces for a non-vacuum black hole.

We also have the same situation for the vacuum black hole. It has $f(0) = -1$ and $f'(0) = 0 = M'(0) = a'(0)$, as required to get the full manifold with two asymptotic regions joined by a "neck" [30]. Note that the vacuum black hole is totally inappropriate for testing Ellis's idea [4], because there are no unique timelike Ricci eigenlines. Generally, for the elliptic case, regions of timelike $S(\tau_c)$ occur outside black holes.

4.4 Discussion

We have found that the $\{\tau=$ constant$\}$ surfaces $S(\tau_c)$ are spacelike everywhere at early times, in both elliptic and hyperbolic cases. However the behaviour of the $S(\tau_c)$ in the two cases can differ at intermediate and late times.

For the hyperbolic models examined, the $\{\tau=$ constant$\}$ surfaces are frequently timelike at the middle times, where equation (3.19) holds, otherwise they become spacelike. At late times they eventually return to being spacelike, except where $M' = f' = 0$, though along worldlines close to this condition the $S(\tau_c)$ surfaces can stay timelike for a long period.

The result is different for elliptic cases. The crunch time must be a constant to get timelike $S(\tau_c)$ at late times. The intermediate times could easily have timelike $S(\tau_c)$ regions.

It is notable that with black hole and black-hole-like models the regions of timelike $S(\tau_c)$ do not occur along worldlines near to the "neck" but they do occur further out.

In all cases, the size of a timelike region is increased by increasing $(-a')$ and vice versa, vanishing completely for samll enough $(-a')$. Additionally, as $(-a')$ decreases, the timelike region shrinks towards the origin.

Chapter 5

Conclusion

The true nature of the past, present and future is a mystery, and how the flow of time can best be represented diagrammatically remains problematic, so there has been a great effort by many authors attempting to envisage the flow of time and give a clear picture of our universe [5–7]. According to the block universe idea [4], the universe consists of a unique family of surfaces $S(\tau)$, and the present is merely one surface of constant τ. Conditions at the present time can be evaluated by integration from known conditions at any earlier time, possibly the beginning, up to the present time. The evolving block universe (EBU) and the crystallising block universe (CBU) take the second law of thermodynamics and quantum effects seriously, and replace the time-reversible, deterministic model with one that recognises the past is fixed while the future is highly mutable [14, 16].

The main purpose of this thesis is to investigate the viability of a particular proposition of Ellis [4], that the correct time τ to use is the proper time along the timelike eignevectors of the Ricci tensor. This τ, we called the "Ricci time". It was suggested that if the resulting constant τ surfaces "sensed" strong gravitational fields, for example by becoming timelike, this would indicate the right kind of behaviour.

The Lemaître-Tolman metric [19–21] was used to generate a variety of models with different features; some like inhomogeneous cosmologies, and some like matter-filled black holes. The slopes of the constant τ surfaces $S(\tau)$ were compared with the slopes of the radial null surfaces in order to determine if they were spacelike, null or timelike.

Analytic methods were used to find conditions for the $S(\tau)$ to become timelike in two limits: early times near to the bang, and late times near to the crunch for elliptic models or $\tau \to \infty$ for hyperbolic models. Intermediate time calculations produced rather complicated results.

Numerical methods were used to calculate and display the full evolution of this relationship for a variety of explicit LT models.

In summary, the $S(\tau)$ surfaces are spacelike everywhere at early times for models that are free of irregularities. This occurs because the bang 3-surface and the $\tau = 0$ 3-surface coincide, and the bang is known to be spacelike.

In the late time limit, the $S(\tau)$ can be timelike, though only under quite strong conditions. These conditions are totally different in hyperbolic and elliptic models. In the hyperbolic case, both the geometry/energy function $f(r)$ and the interior mass function $M(r)$ must be (locally) constant, $M' = 0 = f'$. This means there is vacuum $\rho = 0$ on these worldlines. In the elliptic case, the crunch time must be constant (as it is in FLRW models), even if the bang time is not constant.

We found that timelike $S(\tau)$ regions are common at intermediate times. The "area" of the timelike $S(\tau)$ regions (in the (t, r) plane) strongly depends on $(-a')$. The range and duration of the timelike $S(\tau)$ regions is increased by making $(-a')$ bigger, and if $(-a')$ is sufficiently small the $S(\tau)$ surfaces will be everywhere spacelike. Also as $(-a')$ is decreased, the timelike regions sometimes tend to shrink towards the origin (if there is one).

We note that the condition, $a' = 0$, i.e. a constant bang time, which guarantees all constant Ricci time surfaces are spacelike throughout a model, is also the condition which ensures there are no decaying modes in LT models [45]. The growing and decaying modes have been invariantly characterised in [46]; see [47] for the definitions. The asymptotics of LT models, represented by covariant scalars along radial geodesics, including those with $a' = 0$, were investigated in [48]. Of interest here is the relation to gravitational entropy, which was also investigated for LT models in [49]. They considered the entropy proposals of [50, 51] and a modification of the latter in [52]. They found that entropy grows if there anti-correlations between Hubble and density fluctuations. This requires the decaying modes are sufficiently suppressed, and near the bang they have to be absent for entropy to grow. They also suggest that regions of decreasing entropy and dominant decaying modes may be associated with instability. A related result [53] is that for generic inhomogeneous models, the inhomogeneity initally decreases and then increases, and that entropy decreases while inhomogeneity decreases.

The timelike $S(\tau)$ regions always appeared outside the apparent horizons, i.e. at larger areal radius, though they were often right next to them.

For one specific elliptic model we found there were two discrete timelike $S(\tau)$ regions on certain worldlines, separated by a significant time. One of them was near the past AH and the other was very close to the future AH.

In the black-hole-like models, we found that the timelike regions not only stayed outside the AHs, but also did not occur on worldlines at or near the "neck".

Overall, we found that the Ricci time has the opposite of the suggested behaviour, and if its $\{$constant $\tau\}$ surfaces $S(\tau)$ become timelike, this is in regions outside the apparent horizons, where the gravitational fields are not so strong. Therefore this time may not be appropriate for the EBU.

Appendix A

The Lemaître-Tolman Metric

The Lemaître-Tolman metric [54] is a spherically-symmetric and inhomogeneous dust model with line element

$$ds^2 = -dt^2 + \frac{(R')^2}{1+f}dr^2 + R^2 d\Omega^2, \tag{A.1}$$

where $R(t,r)$ is the real radius and f is a free function determining the local geometry. The Christoffel's symbols are

$$\Gamma^r{}_{tr} = -\Gamma^r{}_{rt} = \frac{\dot{R}'}{R'}, \qquad \Gamma^t{}_{rr} = \frac{R'\dot{R}'}{1+f}, \qquad \Gamma^r{}_{rr} = \frac{R''}{R'}, \tag{A.2}$$

$$\Gamma^\theta{}_{t\theta} = -\Gamma^\theta{}_{\theta t} = \Gamma^\phi{}_{t\phi} = -\Gamma^\phi{}_{\phi t} = \frac{\dot{R}}{R}, \qquad \Gamma^r{}_{\theta\theta} = \frac{(1+F)R}{R'}, \tag{A.3}$$

$$\Gamma^\theta{}_{r\theta} = -\Gamma^\theta{}_{\theta r} = \Gamma^\phi{}_{r\phi} = -\Gamma^\phi{}_{\phi r} = \frac{R'}{R}, \qquad \Gamma^t{}_{\theta\theta} = -R\dot{R}, \tag{A.4}$$

$$\Gamma^\phi{}_{\theta\phi} = -\Gamma^\phi{}_{\phi\theta} = \frac{\cos\theta}{\sin\theta}, \qquad \Gamma^\theta{}_{\phi\phi} = \sin\theta\cos\theta, \tag{A.5}$$

$$\Gamma^t{}_{\phi\phi} = -R\dot{R}\sin^2\theta, \qquad \Gamma^r{}_{\phi\phi} = \frac{(1+f)R\sin^2\theta}{R'}. \tag{A.6}$$

Ricci tensor is given by

$$R_{tt} = -\frac{\ddot{R}'R + 2\ddot{R}R'}{R'R}, \tag{A.7}$$

$$R_{rr} = \frac{R^{'}\left[\ddot{R}^{'}R + 2\dot{R}^{'}\dot{R}\right]}{(1+f)R}, \tag{A.8}$$

$$R_{\theta\theta} = \frac{1}{R^{'}}\left[R\ddot{R}R^{'} + R\dot{R}\dot{R}^{'} + \dot{R}^{2}R^{'} - fR^{'}\right], \tag{A.9}$$

$$R_{\phi\phi} = \frac{1}{R^{'}}\left[\sin^{2}\theta\left(R\ddot{R}R^{'} + R\dot{R}\dot{R}^{'} + \dot{R}^{2}R^{'} - fR^{'}\right)\right]. \tag{A.10}$$

Note that Ricci time [4] is defined as a time a long unique eigenlines for each worldline. This can be measured a long set of timelike eigenlines $x^{a}(\nu)$ of the Ricci tensor, where the 4-velocities $u^{a}(\nu) = dx^{a}(\nu)/dr$ satisfy

$$T_{ab}u^{b} = \lambda_{1}u_{a} \Leftrightarrow R_{ab}u^{b} = \lambda_{2}u_{a}, \tag{A.11}$$

where T_{ab} and R_{ab} are mapping to each other. Einstein tensor is

$$G_{tt} = \frac{1}{R^{2}R^{'}}\left[2R\dot{R}\dot{R}^{'} + \dot{R}^{2}R^{'} - fR^{'}\right], \tag{A.12}$$

$$G_{rr} = -\frac{R^{'2}\left[2R\ddot{R} + \dot{R}^{2} - f\right]}{(1+f)R^{2}}, \tag{A.13}$$

$$G_{\theta\theta} = -\frac{1}{R^{'}}\left[R\left(\ddot{R}R^{'} + \dot{R}^{'}\dot{R} + \ddot{R}^{'}R\right)\right], \tag{A.14}$$

$$G_{\phi\phi} = -\frac{1}{R^{'}}\left[R\sin^{2}\theta\left(\ddot{R}R^{'} + \dot{R}^{'}\dot{R} + \ddot{R}^{'}R\right)\right]. \tag{A.15}$$

The main idea is to solve the zero-Λ Einstein field equations, which are given by

$$G_{\mu\nu} = 8\pi T_{\mu\nu}, \tag{A.16}$$

where $T_{\mu\nu}$ is the energy momentum tensor of (2.2). If $\mu = r$ and $\nu = r$, equation (A.16) reduces to $G_{rr} = 0$ because $T_{rr} = 0$. Thus, (A.13) becomes

$$2R\ddot{R} + \dot{R}^2 = f. \tag{A.17}$$

Multiplying both sides of (A.17) by $\dot{R}$, we get

$$2R\dot{R}\ddot{R} + \dot{R}\dot{R}^2 = f\dot{R}, \tag{A.18}$$

which can be written as

$$\frac{\partial}{\partial t}(R\dot{R}^2) = f\dot{R}. \tag{A.19}$$

Integration of (A.19), gives

$$\dot{R}^2 R = fR + 2M, \tag{A.20}$$

where $M(r)$ is a function of integration. Thus, (A.20) reduces to

$$\dot{R}^2 = \frac{2M}{R} + f. \tag{A.21}$$

The solution of (A.21) depends on the value of f. For the hyperbolic case, where $f > 0$, the conformal time coordinate is defined as

$$R(\eta) = (f)^{1/2}\frac{dt}{d\eta}, \qquad \frac{d\eta}{dt} = \frac{(f)^{1/2}}{R}. \tag{A.22}$$

Then,

$$\dot{R} = \frac{dR}{dt} = \frac{d\eta}{dt}\left(\frac{dR}{d\eta}\right) = \frac{(f)^{1/2}}{R}\left(\frac{dR}{d\eta}\right). \tag{A.23}$$

Substituting (A.23) into (A.21), we find

$$\frac{f}{R^2}\left(\frac{dR}{d\eta}\right)^2 = \frac{2M}{R} + f, \tag{A.24}$$

which can be written as

$$\frac{dR}{d\eta} = \frac{M}{f}\sqrt{\frac{2Rf}{M} + \frac{R^2 f^2}{M^2}} = \frac{M}{f}\sqrt{\left(1 + \frac{Rf}{M}\right)^2 - 1}. \tag{A.25}$$

This means that

$$d\eta = \frac{f dR}{M\sqrt{\left(1+\frac{Rf}{M}\right)^2 - 1}}. \tag{A.26}$$

The solution of (A.26) when $f > 0$ is

$$\eta = \cosh^{-1}\left(1+\frac{Rf}{M}\right) + C, \tag{A.27}$$

where $C = 0$ from the initial condition $\eta = 0$ at $R = 0$. Now, we can rewrite (A.27) as

$$R = \frac{M}{f}(\cosh\eta - 1). \tag{A.28}$$

Substituting (A.28) into (A.22), we find that

$$\frac{M}{f}(\cosh\eta - 1) = (f)^{1/2}\frac{dt}{d\eta}. \tag{A.29}$$

We rearrange (A.29) and integrate, to get

$$t = \frac{M}{f^{3/2}}(\sinh\eta - \eta) + a, \tag{A.30}$$

where $a(r)$ is another function of integration. Thus, (A.30) can be written as

$$(\sinh\eta - \eta) = \frac{f^{3/2}(t-a)}{M}. \tag{A.31}$$

For the parabolic case where $f = 0$, the conformal time coordinate is defined as

$$R(\eta) = \frac{dt}{d\eta}, \qquad \frac{d\eta}{dt} = \frac{1}{R}. \tag{A.32}$$

Then

$$\dot{R} = \frac{dR}{dt} = \frac{d\eta}{dt}\left(\frac{dR}{d\eta}\right) = \frac{1}{R}\left(\frac{dR}{d\eta}\right), \tag{A.33}$$

and substituting (A.33) into (A.21), we find that

$$\frac{1}{R^2}\left(\frac{dR}{d\eta}\right)^2 = \frac{2M}{R}, \tag{A.34}$$

which means that

$$d\eta = \frac{1}{\sqrt{2M}} \frac{dR}{\sqrt{R}}. \tag{A.35}$$

The solution of (A.35) is

$$\eta = \sqrt{\frac{2R}{M}} + C, \tag{A.36}$$

where $C = 0$ from the initial conditions. Now, we can rewrite (A.36) as

$$R = M\left(\frac{\eta^2}{2}\right). \tag{A.37}$$

We substitute (A.37) into (A.32), and we find that

$$M\left(\frac{\eta^2}{2}\right) = \frac{dt}{d\eta}. \tag{A.38}$$

Rearranging (A.38) and integrating, we get

$$t = M\left(\frac{\eta^3}{6}\right) + a, \tag{A.39}$$

and so (A.39) can be written as

$$\left(\frac{\eta^3}{6}\right) = \frac{(t-a)}{M}. \tag{A.40}$$

For the elliptic case, where $f < 0$, the conformal time coordinate is defined as

$$R(\eta) = (-f)^{1/2}\frac{dt}{d\eta}, \qquad \frac{d\eta}{dt} = \frac{(-f)^{1/2}}{R}. \tag{A.41}$$

Then

$$\dot{R} = \frac{dR}{dt} = \frac{d\eta}{dt}\left(\frac{dR}{d\eta}\right) = \frac{(-f)^{1/2}}{R}\left(\frac{dR}{d\eta}\right). \tag{A.42}$$

After substituting (A.42) into (A.21), we find

$$\frac{(-f)}{R^2}\left(\frac{dR}{d\eta}\right)^2 = \frac{2M}{R} + f, \tag{A.43}$$

and this means that

$$d\eta = \frac{-f dR}{M\sqrt{1-\left(1+\frac{Rf}{M}\right)^2}}. \tag{A.44}$$

The solution of (A.44) is

$$\eta = \cos^{-1}\left(1+\frac{Rf}{M}\right) + C, \tag{A.45}$$

where $C = 0$ so that $R(\eta = 0) = 0$. Now, we can rewrite (A.45) in the form

$$R = \frac{M}{(-f)}(1-\cos\eta). \tag{A.46}$$

Finally, substituting (A.46) into (A.41), we find that

$$\frac{M}{(-f)}(1-\cos\eta) = (-f)^{1/2}\frac{dt}{d\eta}. \tag{A.47}$$

Rearranging (A.47) and integrating, we get

$$t = \frac{M}{(-f)^{3/2}}(\eta - \sin\eta) + a. \tag{A.48}$$

and thus (A.48) becomes

$$(\eta - \sin\eta) = \frac{(-f)^{3/2}(t-a)}{M}. \tag{A.49}$$

Appendix B

Parametric Expression for $R'(r, \eta)$

We now derive the parametric expressions needed in chapters 2 and 3 for both elliptic and hyperbolic cases. The derivation for the elliptic case, $f < 0$, is as follows

$$R = \frac{M}{(-f)}(1 - \cos\eta), \tag{B.1}$$

and

$$(\eta - \sin\eta) = \frac{(-f)^{3/2}(t - a)}{M}. \tag{B.2}$$

Differentiating (B.1) with respect to r, we have

$$R' = \frac{M'}{(-f)}(1 - \cos\eta) + \frac{Mf'}{f^2}(1 - \cos\eta) + \frac{M\eta'}{(-f)}\sin\eta. \tag{B.3}$$

Equation (B.2) can be rewritten as

$$t = a + \frac{M}{(-f)^{3/2}}(\eta - \sin\eta), \tag{B.4}$$

and after differentiating (B.4) with respect to r we can find the value of η' from

$$\frac{\partial t}{\partial r} = a' + \frac{M'}{(-f)^{3/2}}(\eta - \sin\eta) + \frac{3}{2}\frac{Mf'}{(-f)^{5/2}}(\eta - \sin\eta) + \frac{M}{(-f)^{3/2}}(1 - \cos\eta)\eta' = 0, \tag{B.5}$$

which gives

$$\eta' = -\frac{(-f)^{3/2}}{M(1 - \cos\eta)}a' - \frac{M'}{M}\frac{(\eta - \sin\eta)}{(1 - \cos\eta)} - \frac{3}{2}\frac{f'}{(-f)}\frac{(\eta - \sin\eta)}{(1 - \cos\eta)}. \tag{B.6}$$

Substitution of (B.6) into (B.3), leads to

$$R' = \frac{M'}{(-f)}\psi_1 + \frac{Mf'}{f^2}\psi_2 + (-a')\sqrt{(-f)}\psi_3, \tag{B.7}$$

where

$$\psi_1 = \frac{2 - 2\cos\eta - \eta\sin\eta}{1 - \cos\eta}, \tag{B.8}$$

$$\psi_2 = \frac{1}{2}\frac{4 - 4\cos\eta - 3\eta\sin\eta + \sin^2\eta}{1 - \cos\eta}, \tag{B.9}$$

and

$$\psi_3 = \frac{\sin\eta}{1 - \cos\eta}. \tag{B.10}$$

The derivation in the hyperbolic case, $f > 0$, follows from

$$R = \frac{M}{f}(\cosh\eta - 1), \tag{B.11}$$

and

$$(\sinh\eta - \eta) = \frac{f^{3/2}(t - a)}{M}. \tag{B.12}$$

Differentiating (B.11) with respect to r, we have

$$R' = \frac{M'}{f}(\cosh\eta - 1) - \frac{Mf'}{f^2}(\cosh\eta - 1) + \frac{M\eta'}{f}\sinh\eta. \tag{B.13}$$

Rewriting (B.12) as

$$t = a + \frac{M}{f^{3/2}}(\sinh\eta - \eta). \tag{B.14}$$

and differentiating it with respect to r gives us

$$\frac{\partial t}{\partial r} = a' + \frac{M'}{f^{3/2}}(\sinh\eta - \eta) - \frac{3}{2}\frac{Mf'}{f^{5/2}}(\sinh\eta - \eta) + \frac{M}{f^{3/2}}(\cosh\eta - 1)\eta' = 0, \tag{B.15}$$

from which we find an expression for η',

$$\eta' = -\frac{f^{3/2}}{M(\cosh\eta - 1)}a' - \frac{M'}{M}\frac{(\sinh\eta - \eta)}{(1 - \cos\eta)} + \frac{3f'}{2f}\frac{(\sinh\eta - \eta)}{(1 - \cos\eta)}. \tag{B.16}$$

We substitute (B.16) into (B.13), and we obtain

$$R' = \frac{M'}{f}\psi_4 + \frac{Mf'}{f^2}\psi_5 + (-a')\sqrt{f}\psi_6, \tag{B.17}$$

where

$$\psi_4 = \frac{2 - 2\cosh\eta + \eta\sinh\eta}{\cosh\eta - 1}, \tag{B.18}$$

$$\psi_5 = -\frac{1}{2}\frac{4 - 4\cosh\eta + 3\eta\sinh\eta - \sinh^2\eta}{\cosh\eta - 1}, \tag{B.19}$$

and

$$\psi_6 = \frac{\sinh\eta}{\cosh\eta - 1}. \tag{B.20}$$

Bibliography

[1] Carlo Rovelli. Forget time. *Foundations of Physics*, 41(9):1475–1490, (2011). URL http://arxiv.org/abs/0903.3832.

[2] Julian Barbour. *The End of Time: The Next Revolution in Phyiscs*. Oxford University Press, (1999).

[3] Paul C. W. Davies. That mysterious flow. *Scientific American Special Edition: A Matter of Time*, 21:8–13, (2012). URL http://www.scientificamerican.com/article/that-mysterious-flow-2012-01/.

[4] George F. R. Ellis. Space time and the passage of time. (2012). URL http://arxiv.org/abs/arXiv:1208.2611.

[5] Jeremy N. Butterfield. The end of time? (2001). URL http://arxiv.org/abs/gr-qc/0103055.

[6] Fqxi forum: The nature of time essay contest. (2014). URL http://www.fqxi.org/community/forum/category/10.

[7] David H. Mellor. *Real Time II*. London: Routledge, (1998).

[8] Huw Price. *Time's Arrow and Archimedes' Point*. Oxford University Press, (1997).

[9] George F. R. Ellis. Cosmology and local physics. *New Astronomy Reviews*, 46(11):645–657, (2002). URL http://arxiv.org/abs/gr-qc/0102017.

[10] Richard P. Feynman, Robert B. Leighton, and Matthew Sands. *The Feynman Lectures on Physics: mechanics, radiation, and heat*. Addison-Wesley, (1963). URL http://www.feynmanlectures.info/.

[11] Richard P. Feynman, Robert B. Leighton, and Matthew Sands. *The Feynman Lectures on Physics: Quantum Mechanics*. Addison-Wesley, (1965). URL http://www.feynmanlectures.info/.

[12] Stephen W. Hawking and George F. R. Ellis. *The Large Scale Structure of Space-Time*. Cambridge University Press, (1973).

[13] George F. R. Ellis and Ruth M. Williams. *Flat and Curved Space Times*. Oxford University Press, Second edition, (2000).

[14] George F. R. Ellis. Physics in the real universe: Time and spacetime. *General Relativity and Gravitation*, 38(12):1797–1824, (2006). URL http://arxiv.org/abs/gr-qc/0605049.

[15] Richard P. Feynman, Robert B. Leighton, and Matthew Sands. *The Feynman Lectures on Physics: electromagnetism and matter*. Addison-Wesley, (1964). URL http://www.feynmanlectures.info/.

[16] George F. R. Ellis and Tony Rothman. Time and spacetime: The crystallizing block universe. *International Journal of Theoretical Physics*, 49(5):988–1003, (2010). URL http://arxiv.org/abs/0912.0808.

[17] George F. R. Ellis. On the limits of quantum theory: Contextuality and the quantum-classical cut. *Annals of Physics*, 327:1890–1932, (2012). URL http://arxiv.org/abs/1108.5261.

[18] Scott Dodelson. *Modern Cosmology*. Academic Press, (2003).

[19] Charles Hellaby. Modelling inhomogeneity in the universe. *Proceedings of Science*, ISFTG: 005, (2009). URL http://arxiv.org/abs/0910.0350.

[20] Andrzej Krasiński. *Inhomogeneous Cosmological Models*. Cambridge University Press, (1997).

[21] Charles Hellaby. Some properties of singularities in the tolman model. *Ph.D. thesis, Queen's University at Kinston, Ontario*, (1985). URL http://www.mth.uct.ac.za/~cwh/CWH_PhD.pdf.

[22] Georges Lemaître. L'univers en expansion. *Annales de la Société Scientifique de Bruxelles*, A53:51–85, (1933).

[23] Richard C. Tolman. Effect of inhomogeneity on cosmological models. *National Academy of Sciences of the USA*, 20:169, (1934).

[24] Hermann Bondi. Spherically symmetrical models in general relativity. *Monthly Notices of the Royal Astronomical Society*, 107:410, (1947).

[25] Roberto A. Sussman. A dynamical system approach to inhomogeneous dust solution. *Classical and Quantum Gravity*, 25:015012, (2007). URL http://iopscience.iop.org/0264-9381/25/1/015012.

[26] Charles Hellaby. The mass of the cosmos. *Monthly Notices of the Royal Astronomical Society*, 370:239–244, (2006). URL http://arxiv.org/abs/astro-ph/0603637.

[27] Charles Hellaby and Alnadhief H. A. Alfedeel. Solving the observer metric. *Physical Review D*, 79:043501, (2009). URL http://arxiv.org/abs/0811.1676.

[28] Krzysztof Bolejko, Andrzej Krasiński, and Charles Hellaby. Formation of voids in the universe within the lemaître-tolman model. *Monthly Notices of the Royal Astronomical Society*, 362:213–228, (2005). URL http://arxiv.org/abs/gr-qc/0411126.

[29] Håvard Alnes, Morad Amarzguioui, and Øyvind Grøn. Inhomogeneous alternative to dark energy? *Physical Review D*, 73(8):083519, (2006). URL http://arxiv.org/abs/astro-ph/0512006.

[30] Charles Hellaby. A kruskal-like model with finite density. *Classical and Quantum Gravity*, 4:635–650, (1987). URL http://iopscience.iop.org/0264-9381/4/3/021.

[31] Andrzej Krasiński and Charles Hellaby. Formation of a galaxy with a central black hole in the lemaître- tolman model. *Physical Review D*, 69:043502, (2004). URL http://arxiv.org/abs/gr-qc/0309119.

[32] George F.R. Ellis. Dynamics of pressure-free matter in general relativity. *Journal of Mathematical Physics*, 8:1171, (1967). URL http://link.aip.org/link/?JMP/8/1171/1&Agg=doi.

[33] Andrzej Krasiński and Charles Hellaby. Structure formation in the lemaître-tolman model. *Physical Review D*, 65:023501, (2001). URL http://arxiv.org/abs/gr-qc/0106096.

[34] Andrzej Krasiński and Charles Hellaby. More examples of structure formation in the lemaître-tolman model. *Physical Review D*, 69:023502, (2004). URL http://arxiv.org/abs/gr-qc/0303016.

[35] Charles Hellaby and Kayll Lake. Shell crossings and the tolman model. *Astrophysical Journal*, 290:381–387, (1985). URL http://adsabs.harvard.edu/full/1985ApJ...290..381H.

[36] Charles Hellaby. The nonsimultaneous nature of the schwarzschild r = 0 singularity. *Journal of Mathematical Physics*, 37:2892, (1996). URL http://scitation.aip.org/content/aip/journal/jmp/37/6/10.1063/1.531545.

[37] José P. S. Lemos. Naked singularities: Gravitationally collapsing configurations of dust or radiation in spherical symmetry, a unified treatment. *Physical Review Letters*, 68:1447–50, (1992). URL http://journals.aps.org/prl/abstract/10.1103/PhysRevLett.68.1447.

[38] Charles Hellaby. On the vaidya limit of the tolman model. *Physical Review D*, 49:6484–6488, (1994). URL http://arxiv.org/abs/gr-qc/9907074.

[39] William B. Bonnor. Closed tolman models of the universe. *Classical and Quantum Gravity*, 2:781–790, (1985). URL http://iopscience.iop.org/0264-9381/2/5/018.

[40] Pankaj S. Joshi. *Global Aspects in Gravitation and Cosmology*. Clarendon Press, Oxford, (1993).

[41] Brad Waugh and Kayll Lake. Shell-focusing singularities in spherically symmetric self-similar spacetimes. *Physical Review D*, 40:2137–2139, (1989). URL https://journals.aps.org/prd/abstract/10.1103/PhysRevD.40.2137.

[42] Richard P. A. C. Newman. Strengths of naked singularities in tolman-bondi space-times. *Classical and Quantum Gravity*, 3:527, (1986). URL http://iopscience.iop.org/0264-9381/3/4/007.

[43] Douglas M. Eardley and Larry Smarr. Time functions in numerical relativity: Marginally bound dust collapse. *Physical Review D*, 19:2239–59, (1979). URL http://journals.aps.org/prd/abstract/10.1103/PhysRevD.19.2239.

[44] Demetrios Christodoulou. Violation of cosmic censorship in the gravitational collapse of a dust cloud. *Communications in Mathematical Physics*, 93:171–95, (1984).

[45] Joseph Silk. Large-scale inhomogeneity of the universe: Spherically symmetric models. *Astronomy and Astrophysics*, 59:53, (1977). URL http://adsabs.harvard.edu/full/1977A%26A....59...53S.

[46] Roberto A. Sussman. Invariant characterisation of the growing and decaying density modes in ltb dust models. *Classical and Quantum Gravity*, 30:235001, (2013).

[47] J. Plebanski and A. Krasinski. *An Introduction to General Relativity and Cosmology*. Cambridge University Press, (2006).

[48] Roberto A. Sussman. Radial asymptotics of lemaître-tolman-bondi dust models. *General Relativity and Gravitation*, 42:2813–2864, (2010). URL http://arxiv.org/abs/1002.0173.

[49] Roberto A. Sussman and Julien Larena. Gravitational entropies in LTB dust models. *Classical and Quantum Gravity*, 31:075021, (2014). URL http://arxiv.org/abs/1310.7632.

[50] Timothy Clifton, George F.R. Ellis, and Reza Tavakol. A gravitational entropy proposal. *Classical and Quantum Gravity*, 30:125009, (2013). URL http://arxiv.org/abs/1303.5612.

[51] Akio Hosoya, Thomas Buchert, and Masaaki Morita. Information entropy in cosmology. *Physical Review Letters*, 92:141302, (2004). URL http://arxiv.org/abs/gr-qc/0402076.

[52] Roberto A. Sussman. Weighed scalar averaging in ltb dust models, part i:statistical fluctuations and gravitational entropy. *Classical and Quantum Gravity*, 30:065015, (2013). URL http://arxiv.org/abs/1209.1962.

[53] Krzysztof Bolejko and William R. Stoeger. Intermediate homogenization of the universe and the problem of gravitational entropy. *Physical Review D*, 88:063529, (2013). URL http://arxiv.org/abs/1309.5695.

[54] Kari Enqvist. Lemaître-tolman-bondi model and accelerating expansion. *General Relativity and Gravitation*, 40(2-3):451–466, (2008). URL http://arxiv.org/abs/0709.2044.